IEEE Access
Multidisciplinary | Rapid Review | Open Access Journal

Received February 25, 2022, accepted March 23, 2022, date of publication April 4, 2022, date of current version April 20, 2022.

Digital Object Identifier 10.1109/ACCESS.2022.3164514

The Selection of Optimal Structure for Stand-Alone Micro-Grid Based on Modeling and Optimization of Distributed Generators

XIAOXU MA[1], SHUQIN LIU[1], HONGTAO LIU[1], AND SIPENG ZHAO[2]
[1]School of Electrical Engineering, Shandong University, Jinan 250061, China
[2]State Grid Liaocheng Electric Power Supply Company, Liaocheng 252000, China

Corresponding authors: Shuqin Liu (lshuqin@sdu.edu.cn) and Xiaoxu Ma (pengfangmingyu@163.com)

This work was supported by the National Key Research and Development Program of China, under Grant 2018YFB2000100.

ABSTRACT The configuration programming of Distributed Generators (DGs) in a micro-grid (MG) through the achievement of multi-objective is an inevitable and primary issue ahead of micro-grid's construction. The motivation of this paper is to select the most suitable catalog of MG from DC micro-grid (DC-MG), AC micro-grid (AC-MG), and hybrid MG by means of uncertainties' models and corresponding DGs' configurations. The DGs in all catalogs of MG are composed of wind turbine (WT), photovoltaic (PV), biomass generation (BG), and battery energy storage (BES) system. In terms of uncertainties' models, the proposed mathematical models are combined with multifarious scenarios which are considered the uncertainties of variations in solar irradiance and wind speed, temperature, and load demand. Particularly, this paper also proposes differences in allocations and sizes of all the equipment based on the assumed specific structure for each catalog of MG. Then, the non-dominated sorting genetic algorithm III (NSGA-III) is utilized by MATLAB working platform to compute the multi-objective functions associating with the minimized system cost, the loss of power supply probability (LPSP), and the greenhouse gas (GHG) emissions for each catalog of MG. Finally, the results and comparisons demonstrate that the AC-MG is the optimal catalog for the case study, which has superiorities of economy and reliability. Although the DC-MG has lower GHG emissions, the AC-MG is the optimal choice after the comprehensive comparisons and analyses depended on three objectives.

INDEX TERMS Distributed generators (DGs), DC micro-grid (DC-MG), AC micro-grid (AC-MG), hybrid micro-grid, the non-dominated sorting genetic algorithm III (NSGA-III).

NOMENCLATURE

A. ABBREVIATIONS

AC-MG	AC micro-grid
BES	Battery Storage System
BG	Biomass generator
DC-MG	DC micro-grid
DGs	Distributed generators
GHG	Greenhouse gas
IGD	Inverted Generational Distance
LPSP	Loss of power supply probability.
MG	Micro-grid
NSGA-III	Non-dominated sorting genetic algorithm III
PV	Photovoltaic
RE	Renewable energy
SOC	State of charge value of the *i*th battery
WT	Wind turbine
CIGS	Copper indium gallium selenium

B. PARAMETERS

b_{bio}	Specific propellant consumption
b_{fuel}	Fuel consumption rate
C_{BES}	Investment cost of BES
C_{BG}	Investment cost of BG
C_{br}	Cost of breaker
C_{ca}	Cost of AC cable
C_{cd}	Cost of DC cable
C_{co}	Cost of converters,
C_{PV}	Investment cost of PV system

The associate editor coordinating the review of this manuscript and approving it for publication was Anamika Dubey.

C_{WT}	Investment cost of wind turbines
f_{PV}	Factor reflecting shading
G_{STC}	Solar irradiation under Standard Test Condition
L	Transport distances from all garbage stations to biomass power generation station
LHV_{fuel}	Low calorific value of fuel
l	Lifetime of DGs
P_{ca}	Rated capacities of AC cables
P_{cd}	Rated capacities of DC cables
P_{co}	Rated capacity of converters
P_r	Rated power of WT
P_{PVr}	Rated power of the PV
$P_{tL}(t)$	Power for transmission lines
T_{STC}	Temperature under Standard Test Condition
r	Discount rate
v_{ci}	Cut-in wind speed
v_{oc}	Cut-off wind speed
v_r	Rated wind speed
η_c	Charging efficiencies of the battery
η_d	Discharging efficiencies of the battery

C. VARIABLES

B_{fuel}	Annual fuel consumption
C_{DE}	Acquisition cost and installation cost of DGs, cables and power electronic devices
C_{DG}	Investment cost of DGs
C_{EQ}	Investment cost of cables and power electronic devices
C_{OM}	Operation and maintenance cost
$C_{OM(DG)}$	Operation and maintenance costs of DGs
$C_{OM(Eq)}$	Operation and maintenance costs of equipment
C_{RE}	Replacement cost of BES and converters
$C_{RE(BES)}$	Replacement cost of BES
$C_{RE(co)}$	Replacement cost of converter
C_T	Minimums of the system cost
C_{TR}	Fuel transportation fee
c	Capital recovery factor
E_{env}	Annual air pollution
$G(t)$	Real solar irradiation
h_{BG}	Annual service hours of biomass generator
I_{av}	Average daily data of illumination intensity
I_{cc}	Duration and frequency of cloud coverage
I_{rand}	Time period of the appearance and disappearance of daily light in different seasons
L_i	Length of DC cable or AC cable
$N_{PV}(i)$	Number of ith PV module
$N_{WT}(i)$	Number of ith wind turbine
P_{BES}	Output power of BES
P_{BG}	Output power of BG
P_c	Charging powers of BES
P_{DG}	Total output power of DGs
P_d	Discharging power of BES
P_{day}	Daily load of residents
P_e	Extra output power in the micro-grid
P_L	Load demand the power required for the load
$P_{PV}(t)$	Output power of PV system
P_{WT}	Actual power of a WT turbine
P_{year}	Annual average daily load
R_{light}	Load of street lamp
$T(t)$	Temperature on panels
V_{dn}	Wind speed of gradient
V_{dn_rand}	The maximum of wind speed at night
V_{gust}	Wind speed of gusts
V_{grad}	Wind speed of gradient
V_{rand}	Random wind speed
v	Actual wind speed
$\boldsymbol{P_{DG}^T}$	Capacity of each DG of each cycle
$\boldsymbol{OP}$	Probability of occurrence
Y	Transportation price
ΔT_{BG}	Average of annual operation hours of BG

I. INTRODUCTION

The primary issue of setting up a micro-grid (MG) is to determine the sizes of distributed generations (DGs) in an MG. A reliable stand-alone MG makes the most of RE resources (wind, PV, hydro [1], biomass [2], geothermal, ocean wave) which show the advantages such as power supply reliability, less GHG emission, and system cost [3]–[5]. Nonetheless, these advantages become kinds of contradictory forces when seeking the multi-objective optimal configuration of DGs in an MG. Based on the contradictions, many latest researches considered different uncertainties such as variations in solar irradiance, wind speed, and load demand to survey the optimal allocations of DGs in an AC-MG, DC-MG, or hybrid MG. However, it is quite under-researched that different catalogs of MG interact with DGs' configurations of MG.

In the last decade, many efforts have been dedicated to the optimization problems of DGs in MGs [6]–[9]. The authors in [10] made use of a refined energy resources management (ERM) system to carry out a DC-MG comprised of PV, micro-turbine, fuel cell, diesel generator, battery system, and load profiles over four seasons of the year. Based on the sizing analysis of DGs in MG, [11]–[13] proposed an optimal sizing approach with comprehensive consideration to find optimal allocations of PV, WT, and battery system in a DC-MG. The NSGA-II algorithm was used to find solutions for a multi-objective problem to minimize the generation cost and to minimize the battery life loss in an isolated AC-MG which consists of wind, PV, diesel generators, and lead-acid batteries [14]. Das and Ni [15] proposed a computationally efficient near- optimal control approach to tackle the problem of optimizing BES systems with other power supply units in islanded AC-MGs, they achieved the minimum daily operational cost. Reference [16] presented an improved Levy-Harmony algorithm with the aid of Levy flight and a triangular aggregation model for a multi-objective optimization scheme of island AC-MGs sizing. Moreover, some researches dealt with the sizing problem of the hybrid MG system that

consists of multiple resources [17]–[19]. Reference [20] carried out a parallel approach combining both PSO and multi-dimensional sensitivity analysis to design the storage optimal sizing in a real island hybrid renewable MG. Also, in order to get an effective integration of DGs within MGs and higher micro-grid performance, reference [21] developed PSO to optimize the control gains of D-FACTS controllers. It is obvious that most of the studies focus on the DGs' configuration optimization in settled AC-MG, DC-MG, or hybrid MG.

Various algorithms are the main method when DGs are organized into MG with reasonable capacity and remarkable energy regulation ability. Certain traditional AI algorithms such as Particle Swarm Optimization (PSO) [18], [22] [23], Genetic Algorithm (GA) [24]–[26] artificial bee colony algorithm (ABC) [27], [28] and ant colony [29] were used for optimization problem with different objectives. The traditional AI algorithms were employed in the early studies and improved in recent years, some studies made comparisons of traditional versions and the improved. The improved particle swarm optimization (IPSO) [30], [31], modified ABC algorithm [32] and improved GA algorithm [33], [34] were proved that have better convergence and excellent dynamic performance than those original visions. For instance, Bao *et al.* [35] proposed an IPSO algorithm with two improvements for solving the coordinated scheduling of day-ahead cooling load and electricity in MG. One improvement was added to the mandatory correction to enhance the algorithm performance. The other one used solution occupation strategy and the size decrease method of near-zero points, which contributed to avoiding the prematurity and showed the superior performance than original PSO. Moreover, some researchers combined two or more algorithms for achieving higher efficiency of optimization in MGs. In [36], the GA algorithm was programmed to look for optimal scheduling of the sources of energy in a grid-connected micro-grid whereas parameters were optimized by Simulated Annealing (SA) method for the optimal scheduling of the sources of energy in a grid-connected micro-grid. In [37], the artificial neural network (ANN) was utilized to evaluate the demand response, meanwhile, the issues of economic dispatch which evaluate the generation. Storage and responsive load offers were solved by bacterial foraging optimization algorithm (BFOA). However, only one or two objective functions were taken into account for the above researches. Recently, researchers gradually considered multi-objective for the sake of various purposes. In order to solve the constrained multi-objective problem, a modified version of GA called Non-dominated Sorting Genetic Algorithm (NSGA) was proposed, and evolutionary versions named NSGA-II [38] and NSGA-III [39], [40] were widely used in optimal scheduling of micro-grid. It was proved that NSGA-III outperforms NSGA-II at working out the multi-objective optimization with three or more objective functions [41], [42]. The NSGA-III was used for the optimization of DGs in a micro-grid [43], [44] to work out the multi-objective functions such as minimum consumption costs, the minimized inconvenience caused by consumers, the rebound peak occurrence, and minimized pollutant emission. Due to the good performance of the multi-objective problem, this paper chooses NSGA-III for solving the optimal issue of configuration in MGs.

Furthermore, the duration, time interval (time step length), and simulation methods of data such as wind speed, solar irradiation, temperature, and load demand were the main uncertainties for most of the research on MG configurations. In [32], an approach combined artificial neural network with a Markov chain (ANN-MC) was used to predict 600 data points of the load demand and power generation of WT and PV during the 24 hours. References [27], [45] determined the WT and PV power values hourly during the 24 hours, and these values were based on the historical data or Predicted data. The authors in [17] showed the historical hourly profile of load and environmental conditions containing the temperature, wind speed, and solar radiation during a year. In [10], the unit power of WT, PV, and the micro-grid's load were considered for a given day in each season of the year. After that, some efforts were focused on forecasting those uncertainties. The study in [46] forecasted average wind speed and loads from 17:05 to18:05 within a day, the forecasted data was obtained from the prediction algorithm and a Real-Time Digital Simulator based on a digital-analog hybrid simulation platform [47]. The study in [48] developed a deep recurrent neural network with long short-term memory units (DRNN-LSTM) model to forecast residential hourly PV power output power and load over short-term horizon respectively. It achieved total costs reduction and system reliability improvement. The mathematical probabilistic models were popular to describe uncertainties as well. In [49], the load demand and solar irradiance were modeled as hourly statistics in a day within one season based on three years of hourly historical data, and the data of solar irradiance was generated by a Beta-probability distribution function (PDF) while the normal PDF was used for the uncertain load demand. These mathematical models contributed to a hybrid system with minimum power losses. Similarly, the method of PDF was employed in [50], [51], Weibull PDF, normal PDF, and Beta PDF were utilized for modeling the uncertainties of the wind speed, load demand, and solar irradiance respectively. A set of scenarios is obtained by a combination of these uncertainties for minimizing the expected power losses.

From the previous surveys, these papers do great work in many aspects of the DGs' configuration of MGs, especially in the improvements of algorithm and uncertainties of the output power of the DGs and load demand. However, differ catalog of MG brought some uncertainties that impact the configuration accuracy of DGs by multi-objective optimal scheduling method, which are considered less. Furthermore, some studies use historical and predicted data in early and most build mathematical models to design solar irradiation, wind speed, and loads. These forms of expression are a bit onefold to describe these uncertainties from diversification. To address this issue, the main innovation points in this article are aware of the following: firstly, this article gives

an in-depth analysis of the uncertainties arisen from different catalogs of MG such as allocation of all the equipment and the prices of converters. Secondly, this paper generates a set of scenarios for solar irradiation, wind speed, and loads, and these scenarios are simulated by mathematical models with smaller time step, which are beneficial for reflecting the randomness.

The motivation of this paper is to select the most suitable catalog of MG and the corresponding optimal capacity size of each DG. On the contrary, it proves that optimization of DGs is the factor that affects the selection of the catalog of MG. the main contributions are as follows:

1) This paper proves that the catalogs of MGs affect the optimal capacity configurations of DGs in an MG. There is little research to substantiate the point. It reminds designers that the uncertainties brought from catalogs of MG should be considered simultaneously with the construction of MG.

2) Many new uncertainties are taken into account when calculating the optimal configuration of DGs in differ catalogs of MG, this conduces to acquire accurate optimal results.

3) Most of the previous works dealt with problems of DGs' configuration after the catalog of MG had been set in advance. Compared with previous works, this paper does not only obtain the optimal configuration of DG as most researches, specifically, it also indicates the most suitable catalog of MG. This prevents the negligence that if researchers calculate the optimal configuration of DG in settled AC-MG, whereas the optimal configuration of DG in hybrid MG are better than that under all setting objective functions unless the AC-MG is obligatory for the project.

This paper is organized as follows: Section II gives a brief introduction of three kinds of micro-grids. In Section III, the output of DGs and BES are modeled. Multi-objective function and constraints are collated in Section IV. Section V shows the NSGA-III algorithm and operating strategy. Section VI shows meteorological models, load models, relative devices, and parameters settings. Section VII and VIII show result analysis and conclusions.

II. THE STRUCTURE OF MICRO-GRIDS

A. DC MICRO-GRID

The alternators are connected to the DC-bus via converters, whereas the AC loads are obtained power from the DC-bus by DC/AC converters. The DC generators and DC loads are connected to the DC-bus via the DC/DC converters. The DC micro-grid has advantages of simple control, lower line loss, it also avoids problems such as frequency, reactive power, and phase.

B. AC MICRO-GRID

The DC generators produced direct current into the AC-bus through the DC/AC converters. The DC loads get power from the AC bus by AC/DC converters. AC generators and AC loads transfer the energy by transformers [52]. Most

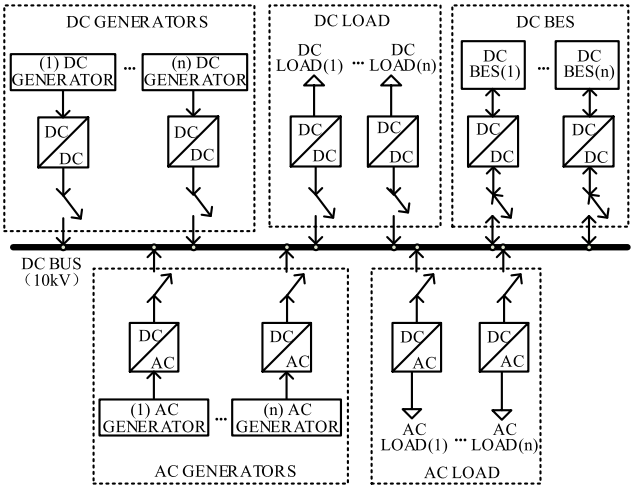

FIGURE 1. The structure of DC micro-grid.

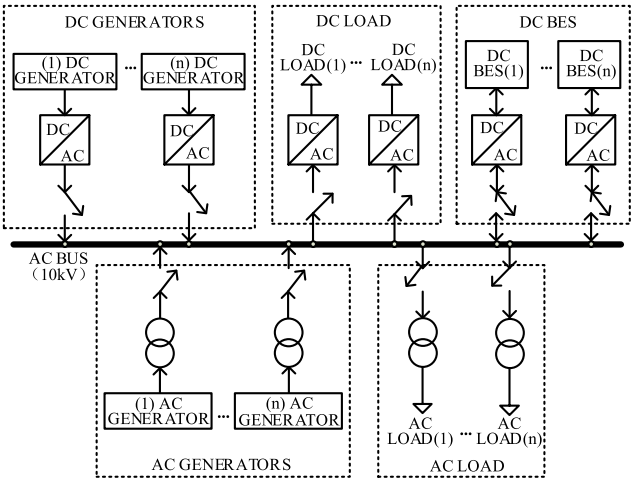

FIGURE 2. The structure of AC micro-grid.

power electronic devices assembled in AC-MG have a more competitive price such as transformers because of mature technologies. However, the shortcomings of an AC micro-grid mainly focus on high line loss, harmonic problems, and control technology.

C. HYBRID MICRO-GRID

A hybrid micro-grid is composed of an AC-MG and a DC-MG, the AC-MG and DC-MG are connected by bidirectional converters [36]. Two bidirectional converters are designed in hybrid MG, this guarantees the power transmission and loads uninterrupted power supply between DC-MG and AC-MG in case either of them gets out of order. The hybrid MG has the characteristics of lower loss, high efficiency, and strong flexibility, whereas it develops other issues such as expensive bidirectional converter [53].

The main differences of the three MGs' structures are significant factors to impact the catalog selection of MG from DC-MG, AC-MG, and hybrid MG. The differences are concluded as follows:

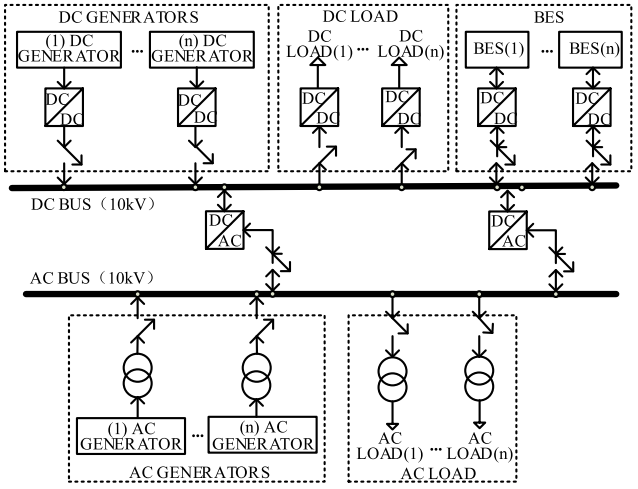

FIGURE 3. The structure of hybrid micro-grid.

1) Bus and electric wire. Each type of micro-grid makes use of different categories, voltage classes, and lengths with regards to bus and electric wire, which has an effect on the capacity configuration optimization of a micro-grid related to the system cost and line loss.

2) Convertors. The choice of convertor is related to the types of current, voltage classes, and capacities of connections including DGs, bus, and loads at the two ends of the convertor. Therefore, the category, number, capacity, and relevant cost of convertors have relationships with the optimization results such as the system cost of capacity configuration optimization.

3) DGs. The capacity and numbers of DGs could be different in each type of micro-grid which affect the total cost and stability of a micro-grid. If the thermal power generation is installed in a micro-grid, the GHG emissions are influenced by the capacity and numbers of thermal power generation. Furthermore, the replacement, operational, and maintenance costs of BES have reduced trend as the technologies matured, the relative parameters are taken into account in this paper.

Thus, the category of MG is an essential consideration for the capacity configuration optimization of a micro-grid.

III. THE MODELS OF DGS

A. OUTPUT POWER OF WT

The power output of a wind turbine is described by a piecewise function as follows [7]:

$$P_{WT}(t)\begin{cases}0, & 0 \le v(t) \le v_{ci}\\ P_r\dfrac{v(t)-v_{ci}}{v_r-v_{ci}}, & v_{ci} \le v(t) \le v_r\\ P_r, & v_r \le v(t) \le v_{oc}\\ 0, & v(t) \ge v_{oc}\end{cases} \quad (1)$$

where v is the actual wind speed at time t, v_{ci}, v_r and v_{oc} represent the cut-in speed, rated wind speed, and cut-off speed separately, P_r denotes the rated power of wind turbine, P_{WT} is the actual power of a WT.

B. OUTPUT POWER OF PV

The maximum power point tracking device (MPPT) is assumed to install in PV system for seeking the maximum solar energy. The output power of the PV system can be described as [54]:

$$P_{PV}(t) = f_{PV} P_{PVr} \frac{G(t)}{G_{STC}}[1 + k(T_{cell}(t) - T_{STC})] \quad (2)$$

where

$$T_{cell}(t) = T(t) + \alpha G(t)(1 + \beta T(t))(1 - \gamma v(t)) \quad (3)$$

where $P_{PV}(t)$ is the output power of PV at time t, f_{PV} is the factor reflecting shading which is set as 0.9 in this paper, P_{PVr} represents the rated power of the PV, G_{STC} and T_{STC} denote solar irradiation and temperature under Standard Test Condition, separately, the value of T_{STC} normally is 25°C, $G(t)$ and $T(t)$ are real solar irradiation and temperature on panels, respectively, k is the temperature coefficient, and $k = -0.0047$°C, $T(t)$ and $v(t)$ represent ambient temperatures and wind speed at time. α, β, and γ are experimental parameters, which are 0.0138, 0.031, and 0.042 respectively.

C. BIOMASS GENERATION SYSTEM

The relationship of fuel consumption and the capacity of BG is shown as:

$$P_{BG} = \frac{B_{fuel}}{b_{fuel} \cdot \Delta T} \quad (4)$$

where P_{BG} represents output power of BG, B_{fuel} is the annual fuel consumption in ton/year, $b_{fuel}$is fuel consumption rate in kg/kWh, ΔT is annual operating hours in a year.

D. BATTERY ENERGY STORAGE SYSTEM

The battery absorbs or releases electrical energy when excess electrical energy or insufficient power exists in the micro-grid. Meanwhile, the BES system in a micro-grid is capable of keeping the power balance, load leveling, and peak shaving. The state of BES is expressed as State-of-Charge (SOC), and it is calculated as [55]:

$$\begin{cases}Discharge: SOC(t+\Delta t) = SOC(t) - \Delta t \cdot P_d(t)/E_{STC} \cdot \eta_d\\ Charge: SOC(t+\Delta t) = SOC(t) + \Delta t \cdot \eta_c \cdot P_c(t)/E_{STC}\end{cases} \quad (5)$$

where $SOC(t)$ is the SOC in the battery at time t, Δt is time steps, $P_c(t)$ and $P_d(t)$ are charging and discharging powers separately, η_c and η_d are charging and discharging efficiencies of the battery, E_B is the nominal capacity of battery.

IV. OBJECTIVE FUNCTIONS AND CONSTRAINTS

A. OBJECTIVE FUNCTIONS

In this paper, the multi-objective function is determined by the minimums of the system cost (C_T), greenhouse gas (GHG) emissions (C_{GHG}) and Loss of Power Supply Probability ($LPSP$). The congregated multi-objective function is shown as:

$$F(X) = min[C_T, C_{env}, LPSP]^T \quad (6)$$

1) THE SYSTEM COST OF MICRO-GRID

The system cost of micro-grid (C_T) should make mention of capital recovery factor (c) which associates with the discount rate (r) and lifetime (l) of DGs or other equipment [31].

$$c = \frac{r\,(1+r)^l}{(1+r)^l - 1} \tag{7}$$

The system cost of micro-grid includes acquisition cost and installation cost C_{DE}, operation and maintenance cost C_{OM}, replacement cost C_{RE} and transportation cost of fuel C_{TR}. C_T is calculated using the following equations:

$$C_T = min \sum [C_{DE} + C_{OM} + C_{RE} + C_{TR}] \tag{8}$$

C_{DE} is nonrecurring investments which includes the purchase cost and installation cost of wind turbines, PV system, BES, BG, cables, and relevant power electronic devices. C_{DE} is expressed as the following equations:

$$C_{DE} = C_{DG} + C_{EQ} \tag{9}$$

where

$$C_{DG} = c \cdot \sum (C_{WT} + C_{PV} + C_{BG} + C_{BES}) n_{i,j} P_{i,j}^{max} \tag{10}$$

$$C_{EQ} = c \cdot \left[\sum_{i=0}^{n} (C_{ca} + C_{cd})\, L_i + \sum_{i'}^{n'} (C_{br} + C_{co}) n_{i'} P_{i'}^{max} \right] \tag{11}$$

where C_{DG} and $C_{EQ}$are investment cost of DGs and equipment investment cost separately,C_{WT}, C_{PV}, C_{BG}, and C_{BES} are the investment cost of wind turbines, PV system, BG and BES, C_{ca} and C_{cd} indicate the investment of AC cable and DC cable in the micro-grid, C_{br} and C_{co} are the cost of breaker and converters, respectively, $n_{i,j}$ is the number of each DG, i is the ith type of DGs, j denotes the jth type in the same DG, for example, the number of the second type of PV is written as $n_{PV,2}$ or $n_{1,2}$. i and j also represent the positions in a matrix, $n_{i'}$ is the number of the i'th equipment, P_i^{max} indicates the maximum capacity of the i,jth equipment such as $P_{WT,1}^{max}$ and $P_{PV,2}^{max}$, L_i is the length of DC cable or AC cable.

This paper adopts the capital recovery factor to calculate the C_{OM}, C_{RE} and C_{TR} in every year. C_{OM} is made up of the operation and maintenance costs of DGs $C_{OM(DG)}$ and equipment $C_{OM(Eq}$, which is shown as follows:

$$C_{OM} = c \cdot \left(C_{OM(DG)} + C_{OM(Eq)}\right) \tag{12}$$

where

$$C_{OM(DG)} = c \cdot \int_0^t [k_{WT} P_{WT}(t) + k_{PV} P_{PV}(t) + k_{BG} P_{BG}(t) + k_{BES} |P_{BES}(t)|] dt \tag{13}$$

$$C_{OM(Eq)} = c \int_0^t [k_{ca} P_{ca}(t) + k_{cd} P_{cd}(t) + k_{co} P_{co}(t)] dt \tag{14}$$

where k_{WT}, k_{PV}, k_{BG}, k_{BES}, k_{ca}, k_{cd} and k_{co} demonstrate the coefficients of operational and maintenance cost of WT, PV, BG, BES, AC cable, DC cable, and converters, $P_{ca}(t)$ and $P_{cd}(t)$ are the rated capacities of AC cables and DC cables separately, $P_{co}(t)$ represents the rated capacity of converters.

Replacement cost is the investment which is used for changing DGs or equipment when DGs or equipment are damaged during the life-cycle of the micro-grid. Generally, the lifetime of BES and converters are usually less than 20 years [56]. Therefore, the system needs to consider the replacement of them for guarantying system normal operation during the whole lifetime. C_{RE} can be formulated as [44]:

$$C_{RE} = (C_{RE(BES)} + C_{RE(co)}) \sum_{k=1}^{k_0} r_k \times [\sum_{l=0}^{l_k} \left(\frac{(1+i_{k1})(1+i_{k2})}{1+r} \right)^{l \cdot n_k}] \tag{15}$$

where C_{RE} denotes the total replacement cost including BES and converters, $C_{RE(BES)}$ and $C_{RE(co)}$ are the replacement cost of BES and converters separately, r_k is the cost coefficient of the kth battery, k_0 is the number of types of battery in BES system, i_{k1} and i_{k2} are the annual increase rate of replacement costs and the rate of cost reduction caused by technological innovation, respectively, n_k is the lifetime of the kth energy storage device.

C_{TR} is caused by fuel transport from all garbage stations to biomass power generation station. It relates to annual fuel consumption (B_{fuel}), transportation price (Y), and transport distances (L).

$$C_{TR} = B_{fuel} YL \tag{16}$$

where B_{fuel} is shown as [57]:

$$B_{fuel} = b_{bio} \int_0^t P_{BG}(t) \mathrm{d}t = b_{bio} P_{BG} h_{BG} \tag{17}$$

where b_{bio} is specific propellant consumption in kg/kWh, h_{BG} represents the annual service hours of biomass generator.

2) LOSS OF POWER PROBABILITY

The LPSP reflects the reliability of the micro-grid system. That ensuring the DGs power meets the load demand is the main purpose of the micro-grid system. The lower LPSP indicates that the power supply of DGs in the micro-grid is much more able to satisfy the loads' needs. The expression of LPSP is as follows [17]:

$$LPSP = \min \left[\frac{\sum_{t=1}^{8760} [P_{DG}(t) - P_L(t)]}{\sum_{t=1}^{8760} [P_L(t)]} \right] \tag{18}$$

where $P_{DG}(t)$ is the total output power of $P_{WT}(t)$, $P_{PV}(t)$, P_{BG} and $P_{BES}(t)$, $P_{BES}(t)$ is the output power of BES, P_L denotes the load demand.

3) ANNUAL AIR POLLUTION

The air pollution is mainly emitted by BG, and the pollutants include: CO_2, CO, SO_2, NO_x and dust. Meanwhile, the amounts of pollutants are proportional to the output power of BG and the operating time [45].

$$E_{env} = min[\Delta T_{BG} \sum_{i \in K} v_i \cdot P_{BG}] \tag{19}$$

where v_i is the amount of ith pollutant in kg/kWh, K is the species number of pollutants, ΔT_{BG} is the average annual operation hours of BG.

B. SYSTEM CONSTRAINTS

1) POWER BALANCE CONSTRAINT

The output power of DGs needs to match the power of load and other requirements in the micro-grid. At the same time, the power balance is obliged to keep in a state of equilibrium during the whole life cycle of the micro-grid [18]:

$$P_L(t) + P_{tL}(t) + P_e(t) = P_{WT}(t) + P_{PV}(t) + P_{BG}(t) + P_{BES}(t) \quad (20)$$

where $P_L(t)$ is the power required for the load, $P_e(t)$ is the extra output power in the micro-grid, $P_{tL}(t)$ is the power for transmission lines which consists of DC cable and AC cable.

$$P_{tL}(t) = P_{ca}(t) + P_{cd}(t) \quad (21)$$

$$P_e(t) = P_{WT}(t) + P_{PV}(t) + P_{BG}(t) + P_{BES}(t) - P_L(t) - P_{tL}(t) \quad (22)$$

2) CONSTRAINTS OF WT

Technically, the power output and permissible number of WTs are limited by lower and upper limits [10]:

$$0 \le N_{WT(i)} \le N_{WT(i)}^{max} \quad (23)$$

$$P_{WT(i)}^{min} \le P_{WT(i)}(t) \le P_{WT(i)}^{max} \quad (24)$$

where $N_{WT(i)}$ is the number of ith wind turbine, $N_{WT(i)}^{max}$ represents the maximum number of ith wind turbine, $P_{WT(i)}^{min}$ and $P_{WT(i)}^{max}$ are the minimum and maximum output power of ith wind turbine, $P_{WT(i)}(t)$ denotes the output power of ith wind turbine.

3) CONSTRAINTS OF PV [18]

$$0 \le N_{PV(i)} \le N_{PV(i)}^{max} \quad (25)$$

$$P_{PV(i)}^{min} \le P_{PV(i)}(t) \le P_{PV(i)}^{max} \quad (26)$$

where $N_{PV(i)}$ is the number of ith PV module, $N_{PV(i)}^{max}$ represents the maximum number of ith PV module, $P_{PV(i)}^{min}$ and $P_{PV(i)}^{max}$ are the minimum and maximum output power of ith PV module, $P_{PV(i)}(t)$ denotes the output power of ith PV module.

4) BES CONSTRAINTS [18]

$$SOC_i^{min} \le SOC_i(t) \le SOC_i^{max} \quad (27)$$

$$P_{ch,BES(i)}(t) \le P_{ch,BES(i)}^{max} \quad (28)$$

$$P_{dis,BES(i)}(t) \le P_{dis,BES(i)}^{max} \quad (29)$$

where $SOC_i(t)$ is the state of charge value of the ith battery, SOC_i^{min} and SOC_i^{max} are the minimum and maximum SOCs of the ith battery, respectively, $P_{ch,BES(i)}(t)$ and $P_{dis,BES(i)}(t)$ indicate the charging and discharging power of ith battery, $P_{ch,BES(i)}^{max}$ is the maximum capacity limit of the charging power in the ith battery, $P_{dis,BES(i)}^{max}$ is the maximum capacity limit of the discharging power of ith battery. In this paper, the BES charges or discharges when SOC(t) is within certain ranges. When the SOC of the battery reaches the upper limit SOC_i^{max}, the battery would not be charged anymore. On the contrary, the battery would not discharge if the SOC of the battery is lower than SOC_i^{min}. It is necessary to mention that charge and discharge power in an hour should no more than 20% of the capacity of battery.

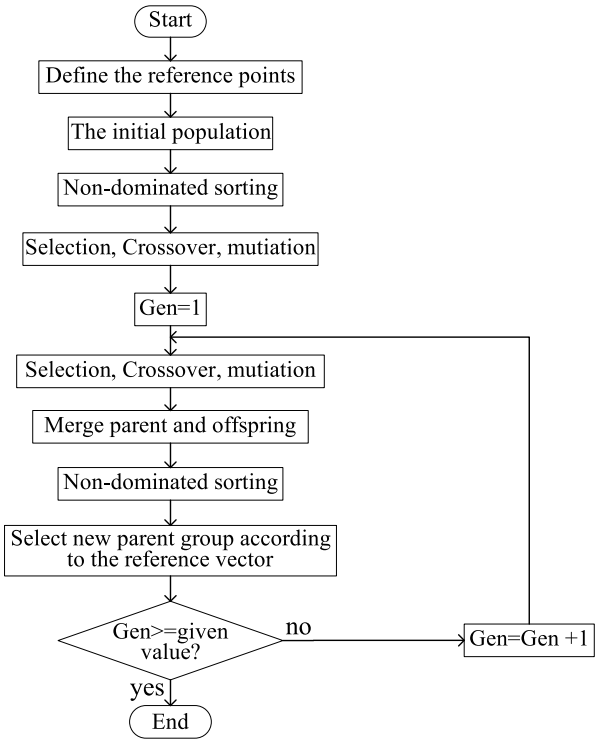

FIGURE 4. The flowchart of the NSGA-III algorithm.

5) CONSTRAINTS OF BG

The power output of BG should be between max and min boundaries, as follow [18]:

$$P_{BG}^{min} \le P_{BG}(t) \le P_{BG}^{max} \quad (30)$$

where P_{BG}^{min} and P_{BG}^{max} are the minimum and maximum output power of BG.

V. ALGORITHM, OPERATING STRATEGY, AND PARAMETERS OF DGS

A. NSGA-III ALGORITHM

In this paper, the NSGA-III algorithm is used for handling multi-objective optimization problems. The NSGA-III has outstanding performance when it faces up to optimization problems composed of three or more objectives [43]. In particular, the diversity of candidate solutions is aided by a number of well-spread reference points which result in a very uniform distribution of Pareto solutions in the search space, even when the number of objectives is large [40]. The flowchart of the NSGA-III algorithm is shown in Figure 4.

The number of individuals in the population is set as 200. However, 190 non-dominated optimal solutions and corresponding optimal schemes can be obtained after 200 iterations because of the recursive method. The NSGA-III is used to calculate the optimal capacities' schemes of DGs in the three types' micro-grid.

B. THE OPERATING STRATEGY

The operating strategy of isolated micro-grids is as follows:

Step 1: The BG stops running when the output power of RE meets the load demand. If the SOC of BES is less than SOC^{max} as well as the excess power in the micro-grid is less than the maximum charging power $P_{ch,BES}^{max}$, the BES gets on charging.

Step 2: When the excess power in MG exceeds $P_{ch,BES}^{max}$ of the BES or the SOC of BES is greater than SOC^{max}, the BES rejects to charge. Meanwhile, the WTs or PVs get power reduction.

Step 3: When the RE could not meet the load demand and $P_{BG}^{min} \le P_L - P_{WT} - P_{PV} \le P_{BG}^{max}$, the BG turns on but the BES does not charge and discharge.

Step 4: If $P_L - P_{WT} - P_{PV} < P_{BG}^{min}$ and SOC of BES is less than SOC^{max}, and the value of $(P_{BG}^{min} - P_L + P_{WT} + P_{PV})$ is less than $P_{ch,BES}^{max}$, the BG starts on with P_{BG}^{min}, and BES is charged.

Step 5: If the output power of BG is lower than P_{BG}^{min} but BES does not satisfy the charging conditions, the RE power generation will have a power reduction and the output power of BG is P_{BG}^{min}.

Step 6: When the output power of BG is at P_{BG}^{max}, however, the output power of the RE and BG still cannot satisfy the load demand, the BES discharges if the BES meets the discharge conditions.

Step 7: When the output power of BG is at P_{BG}^{max}, however, the output power of the RE and BG still cannot satisfy the load demand. If the SOC of BES is less than SOC^{max}, and the value of $(P_L - P_{WT} - P_{PV} - P_{BG}^{max})$ is larger than $P_{dis,BES}^{max}$, the BES discharges with $P_{dis,BES}^{max}$ at this moment. Meanwhile, LPSP is recorded.

Step 8: When the output power of BG is at P_{BG}^{max}, however, the output power of the RE and BG still cannot satisfy the load demand. If the SOC of BES and the value of $(P_L - P_{WT} - P_{PV} - P_{BG}^{max})$ are larger than SOC^{max} and $P_{dis,BES}^{max}$ respectively, the algorithm records the LPSP directly.

VI. CASE STUDY

The Kongtong Island of 37°56′ north latitude and 121°52′ east longitude. The Kongtong Island is located in the east of China and 10 kilometers away from the mainland, which is rich in wind and light but electricity.

In this paper, the history data of wind speed, temperature, and illumination intensity on Kongtong Island are get from the NASA data station. These historical data are daily average, and cannot reflect the characteristics of randomness, intermittent, and mutability. Therefore, this paper establishes environmental uncertainties based on history data by MATLAB. The time step and duration of data are set as 0.1 hours and 8,760 hours separately, which are better to restore the real fluctuation and benefit to the accuracy of optimal results. Besides, the uncertainties of devices are also described in this section.

A. WIND SPEED

The model of wind speed is divided into two parts, deterministic wind speed, and nondeterministic wind speed. The deterministic wind speed is dependent on historical wind speed data (V_{av}) which is shown in Figure 5(a). It describes the distribution trend of wind resources in a year. The nondeterministic wind speed including gust, gradient wind, random wind, and day-night wind speed differences are designed in the random wind speed.

Normally, the wind speed at night is higher than that during the day. The differences in wind speed between day and night (V_{dn}) is shown in Figure 5 (b). it is formulated as [58]:

$$V_{dn} = \begin{cases} 0, & t < t_{dn1} \ or \ t > t_{dn2} + t_{dn4} \\ V_{dn\_rand} \dfrac{t - t_{dn1}}{t_{dn2} - t_{dn1}}, & t_{dn1} \le t \le t_{dn2} \\ V_{dn\_rand}, & t_{dn2} < t \le t_{dn2} + t_{dn3} \\ V_{dn\_rand} \dfrac{t - t_{dn3}}{t_{dn4} - t_{dn3}}, & t_{dn3} \le t \le t_{dn4} \end{cases} \tag{31}$$

where V_{dn} represents the wind speed of gradient, V_{dn_rand} is the maximum wind speed at night, t_{dn1} represents the beginning of night wind, t_{dn2} represents the ending of the night wind, t_{dn3} is the period of the night wind, t_{dn4} represents the ending of the night wind.

The gusts are shown in Figure 5(c) and formulated as [58]:

$$V_{gust} = \begin{cases} 0, & t < t_1 \\ \dfrac{V_{gust\_max}}{2} \left\{ 1 - cos \left[2\pi \left(\dfrac{t - t_1}{T_{gust}} \right) \right] \right\}, & t_1 \le t \le t_1 + T_{gust} \\ 0, & t_1 + T_{gust} \le t \end{cases} \tag{32}$$

where V_{gust} is the wind speed of gusts, V_{gust_max} is the maximum of gusts, t_1 represents the beginning of the gusts, T_{gust} is the period of gusts.

The gradient wind is shown in Figure 5(d) and formulated as:

$$V_{grad} = \begin{cases} 0, & t < t_{grad1} \ or \ t > t_{grad2} + t_{grad3} \\ V_{grad\_max} \dfrac{t - t_{grad1}}{t_{grad2} - t_{grad1}}, & t_{grad1} \le t \le t_{grad2} \\ V_{grad\_max}, & t_{grad2} < t \le t_{grad2} + t_{grad3} \end{cases} \tag{33}$$

where V_{grad} represents the wind speed of gradient, V_{grad_max} is the maximum gradient wind speed, t_{grad1} represents the beginning of gradient wind speed, t_{grad2} represents the ending of gradient wind speed, t_{grad3} is the period of gradient wind speed.

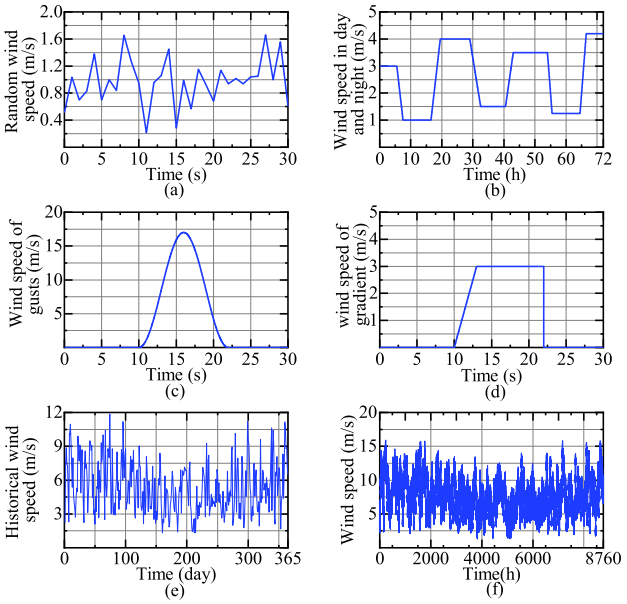

FIGURE 5. The model of wind speed.

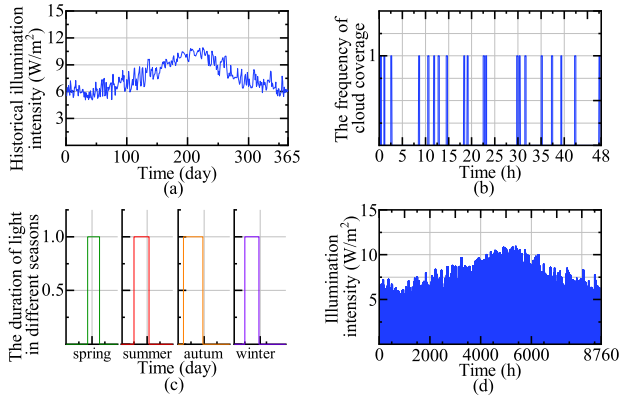

FIGURE 6. The model of illumination intensity.

The random wind is shown in Figure 5(e) and formulated as:

$$V_{rand} = V_{rand\_max} * R\,(-1, 1) * \cos(\omega_n t + \varphi_n) \quad (34)$$

where V_{rand} and V_{rand_max} are random wind and its maximum value, $R\,(-1, 1)$ denotes the random value between 0 and 1, ω_n represents the average value of random wind, normally between 0.5 and 2rad/s, φ_n is the random value between 0 and 2π.

The total wind speed ($v(t)$) is assembled by the whole scenario, which is shown in Figure 5(f).

$$v\,(t) = V_{gust} + V_{grad} + V_{rand} + V_{dn} + (V_{av} - 5rand) \quad (35)$$

B. ILLUMINATION INTENSITY

The photovoltaic power is based on the historical data of illumination intensity (I_{av}) shown in Figure 6(a). Besides, it also supplements some special situations such as cloud coverage and the duration of sunlight affected by the season.

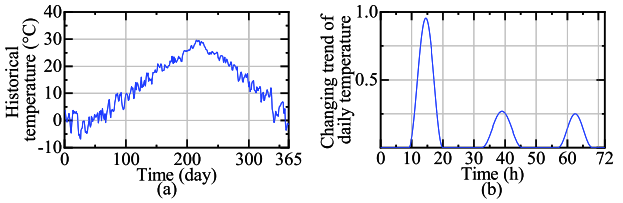

FIGURE 7. The model of temperature.

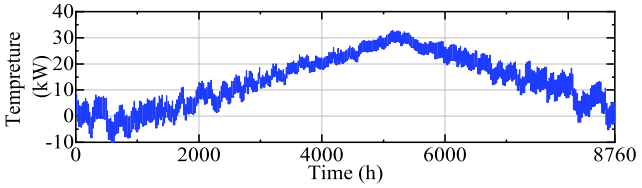

FIGURE 8. The model of simulated temperature.

The scenario of cloud coverage shows the duration and frequency of cloud coverage (I_{cc}), and it is described in Figure 6(b) and formulated as:

$$I_{cc} = \begin{cases} 0, & t < t_{cc1} \text{ or } t > t_{cc1} + \Delta t \\ 1, & t_{cc1} \le t \le t_{cc1} + \Delta t \end{cases} \quad (36)$$

where t_{cc1} represents the beginning of cloud coverage, Δt is the period of cloud coverage.

The duration of sunlight in different seasons (Figure 6(c)) shows the time period of the appearance and disappearance of daily sunlight (I_{rand}). The equations are expressed as:

$$I_{rand} = \begin{cases} 0, & t < t_{ra1} \text{ or } t > t_{ra2} \\ 1, & t_{ra1} \le t \le t_{ra2} \end{cases} \quad (37)$$

where t_{ra1} is the beginning of daytime illumination intensity, t_{ra2} represents the ending of daytime illumination intensity.

The total illumination intensity ($G(t)$) is shown in Figure 6(d) and formulated as:

$$G(t) = (I_{av} - I_{cc} * I_{av}) * I_{rand} \quad (38)$$

C. TEMPERATURE

The temperature is introduced for the precise calculation of PVs' output power. The simulated temperature is a combination of historical data (Figure 7(a)) and changing trend of daily temperature (Figure 7(b)).

In fact, the temperature has certain differences at different times of a day. The changing trend of daily temperature (T_{day}) can be calculated as:

$$T_{day} = \frac{Rand(0, 1)}{2} \left\{ 1 - cos \left[2\pi \left(\frac{t - t_{day}}{\Delta T_{day}} \right) \right] \right\} \quad (39)$$

where t_{day} represents the beginning of T_{day}, ΔT_{day} is the period of T_{day}.

The simulated temperature is shown in Figure 8.

The total temperature is shown as:

$$T_{total} = T_{av} * \left(1 + (T_{day} - 0.5)\right) \quad (40)$$

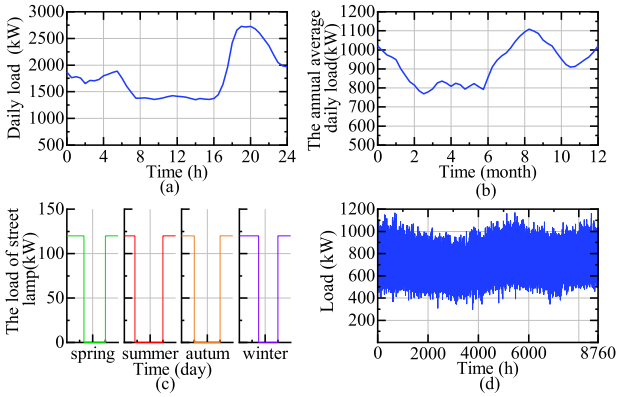

FIGURE 9. The model of loads.

D. LOAD MODEL

The load on Kongtong Island is divided into three scenarios: the annual average daily load of residents, daily load of residents, and the load of street lamp. The annual average daily load (P_{year}) and daily load of residents (P_{day}) are historical data, which are shown in Figures 9(a) and 9(b).

The street lamps are turned on and off at different times in different seasons. The load of street lamp is calculated as:

$$R_{light} = \begin{cases} 0, & t < t_{light1} \ or \ t > t_{light2} \\ 120, & t_{light1} \leq t \leq t_{light2} \end{cases} \tag{41}$$

where t_{light1} is the beginning of street lamp, t_{ra2} represents the ending of street lamp.

The total load model $R_{total}(d, t)$ is expressed as:

$$R_{total}(d, t) = a * P_{year}(d) + b * P_{day}(t) + R_{light} \tag{42}$$

where a and b are the weights of the annual average loads and daily loads of residents, respectively, in addition, $a + b = 1$. P_{yaer} is the annual average loads of residents, P_{day} indicates the daily load of residents, d represents the dth day in a year, t donated the of a day.

E. SELECTION AND PARAMETERS OF EQUIPMENT

For the sake of better selection of DGs, this paper takes many types of DGs into consideration. The parameters of different DG are significant information to affect the final result of populations. It is helpful when the designers cannot estimate the applicability of one type of DG.

1) PHOTOVOLTAIC MATERIAL

Pc-Si cells have a slight advantage in price but the conversion efficiency is mediocre. Cs-Si cells have the highest conversion efficiency than the other two types, but the price is relatively higher. The thickness of CIGS thin-film solar cells is only 1μm, which can be attached to the roof because of its good toughness. The parameters of PV are listed in Table 1.

2) WIND TURBINES

The cost of a wind turbine increase with the growth of the capacity of wind turbine. Nevertheless, the unit costs of construction and transportation decrease with the increase of capacity of a WT. Considering the difficulties in transport, the WTs larger than 500kW are not considered. The capacity of wind turbines and relevant technical parameters are listed in Table 2.

TABLE 1. Parameters of photovoltaic material.

photovoltaic material	Cost（￥/W）	Voltage(V)/ Capacity(W)	conversion efficiency
Sc-Si Cell	2.80	36/300	18%~25%
Pc-Si cells	2.75	300	14%~20%
CIGS	6	300	10%

TABLE 2. Parameters of wind turbines.

installed capacity	Cost ￥/kW	carriage /incidental cost ￥/kW	construction cost ￥/kW	installation cost ￥/kW
110kW	12800	200	13800	800
250kW	10500	200	11500	800
330kW	10300	200	11300	800
500kW	8500	200	9500	800

TABLE 3. Parameters of batteries.

Battery	Cost ￥/Wh	Density Wh/kg	deep discharge	cycles
lead-acid battery	0.8	28	0.4	700
ternary lithium battery	2.7	165	0.2	3500

3) BATTERIES

The lead-acid battery and ternary lithium battery's relevant technical parameters are listed in Table 3.

4) BIOMASS POWER GENERATION

The fuel cost is a significant factor in biomass power generation. The annual consumption of fuels is linearly associated with the capacity of BGs. According to formula (4), the fuel consumption rate (b_{fuel}) is calculated as [57]:

$$b_{fuel} = \frac{3600}{LHV_{fuel} \cdot \eta_e} \tag{43}$$

where LHV_{fuel} is the low calorific value of fuel, $LHV_{fuel} = 4600$kcal/kg, η_e represents generating efficiency in 44%.

The annual per capita waste output is about 440kg/year, and the number of residents on the island is around 1000. Thus, b_{fuel} and the annual consumption of biomass fuel are 1.78kg/kWh and 440t respectively.

The operation of BG results in GHG emissions. The contamination caused by these emissions are assessed as shown in Table 4.

5) POWER ELECTRONIC DEVICES

There are different types of power electronic devices installed in DC-MG, AC-MG, and hybrid MG. The costs of those devices affect the total cost in different MG. Besides, the

TABLE 4. Parameters of biomass power generation.

GHG	SO_2	NO_X	CO_2	CO	Dust
Emmision g/kW·h	0.5	3	320	0.14	2

voltage level, amount and capacity of these devices also have effects on the economics and the result of the optimized configuration in different MGs. The prices of the devices are shown in Table 5. Based on the structure models of AC-MG, DC-MG, and MG, Table 6 shows the number of different electronic devices and lengths of cables in the three types of MG. These reflect the uncertainties in different structures of MG.

F. PROGRAMMING

The population is given as the number of different types of DGs. $\boldsymbol{X_n}$ and $\boldsymbol{P_{DG}^T}$ are populations and capacity of each DG when the program runs at $\boldsymbol{n}$th cycles,which are shown as (44) and (45), at the bottom of the page, where $\boldsymbol{P_{PV}^T}$, $\boldsymbol{P_{WT}^T}$, $\boldsymbol{P_{bes}^T}$ and $\boldsymbol{P_{BG}^T}$are the matrices of capacities of PV, WT, BES, and BG, respectively.

Some calculations involve the tensor product function of '*kron*' in MATLAB software. This function is used to realize the product of different scale matrices. Taking the costs of DGs as an example:

$$\boldsymbol{C_{DG}} = \begin{bmatrix} \boldsymbol{C_{PV}} & \boldsymbol{C_{WT}} & \boldsymbol{C_{bes}} & \boldsymbol{C_{BG}} \end{bmatrix} \tag{46}$$

where

$$\boldsymbol{C_{PV}} = \begin{bmatrix} C_{PV}^1 & C_{PV}^2 & C_{PV}^3 \end{bmatrix} \tag{47}$$

$$\boldsymbol{C_{WT}} = \begin{bmatrix} C_{WT}^1 & C_{WT}^2 & C_{WT}^3 \end{bmatrix} \tag{48}$$

$$\boldsymbol{C_{bes}} = \begin{bmatrix} C_{bes}^1 & C_{bes}^2 \end{bmatrix} \tag{49}$$

$$\boldsymbol{C_n} = \boldsymbol{kron}((\boldsymbol{X_n} .* \boldsymbol{P_n^T}), \boldsymbol{C_{DG}}) = [C_n^1 C_n^2 \dots C_n^N] \tag{50}$$

where $\boldsymbol{C_{DG}}$ is the matrix combined by the matrices $\boldsymbol{C_{PV}}$, $\boldsymbol{C_{WT}}$, $\boldsymbol{C_{bes}}$, and $\boldsymbol{C_{BG}}$ which are the unit costs of various types of DGs, $\boldsymbol{C_n}$ is the total cost of DGs in each individual of population.

It is necessary to record the running time of different DGs during the operating cycle of a micro-grid. The running time of each DG is related to the probability of occurrence ($\boldsymbol{OP}$) in every moment. The $\boldsymbol{OP}$ is recorded as true (1) when the DG is running (on). On the contrary, it is recorded as false (0) when the DG is stopped (off). The values in matrix $\boldsymbol{OP}$ are modified on the basis of $\boldsymbol{OP_{ini}}$. The DGs' annual $\boldsymbol{OP_{ini}}$ with 0.1 steps is shown in Algorithm 1.

$$\boldsymbol{OP_{ini}} = \begin{bmatrix} T_{PV1}^1 & T_{PV1}^2 & \dots & T_{PV1}^{87600} \\ T_{PV2}^1 & T_{PV2}^2 & \dots & T_{PV2}^{87600} \\ T_{PV3}^1 & T_{PV3}^2 & \dots & T_{PV3}^{87600} \\ T_{WT1}^1 & T_{WT1}^2 & \dots & T_{WT1}^{87600} \\ \vdots & \vdots & \ddots & \vdots \\ T_{WT4}^1 & T_{WT4}^2 & \dots & T_{WT4}^{87600} \\ T_{bes1}^1 & T_{bes1}^2 & \dots & T_{bes1}^{87600} \\ T_{bes2}^1 & T_{bes1}^2 & \dots & T_{bes2}^{87600} \\ T_{BG}^1 & T_{BG}^2 & & T_{BG}^{87600} \end{bmatrix} \tag{51}$$

where the elements in $\boldsymbol{OP_{ini}}$ denote the probability of occurrence of each DG based on the meteorological model.

According to the operating strategy, the value of a DG in $\boldsymbol{OP}$ extracts the accordingly value in $\boldsymbol{OP_{ini}}$ when the operating state presented in $\boldsymbol{OP_{ini}}$ is same as the actual running status of DG, otherwise, it flips the accordingly value in $\boldsymbol{OP_{ini}}$ between 0 and 1. For example, when the value of WT2 in $\boldsymbol{OP_{ini}}$ is 1, whereas WT2 suffers power reduction and stops running, thus the value of WT2 in the $\boldsymbol{OP}$ will be flipped 1→0. The program flow of DGs' annual $\boldsymbol{OP}$ with 0.1 steps is shown in Algorithm 2.

The annual running time of each DG is determined by $\boldsymbol{OP}$, the total output power of DGs, and load demand. Taking BG as an example, the annual running time of BG in the program flow of running time is formulated as:

$$\boldsymbol{T_{BG}^n} = \boldsymbol{0.1} * \sum_{t=0}^{87600} \boldsymbol{OP_{BG}^t} \tag{52}$$

where $\boldsymbol{T_{BG}^n}$ is the annual running time of BES in the whole year of a micro-grid at $\boldsymbol{n}$th cycles, $\boldsymbol{OP_{BG}^t}$ is the operating probability of each step. The step is set as 0.1.

$$\boldsymbol{X_n} = \begin{bmatrix} X_{PV1}^1 & X_{PV2}^1 & X_{PV3}^1 & X_{WT1}^1 & \dots & X_{WT4}^1 & X_{bes1}^1 & X_{bes2}^1 & X_{BG}^1 \\ X_{PV1}^2 & X_{PV2}^2 & X_{PV3}^2 & X_{WT1}^2 & \dots & X_{WT4}^2 & X_{bes1}^2 & X_{bes2}^2 & X_{BG}^2 \\ \vdots & \vdots & \vdots & \vdots & \ddots & \vdots & \vdots & \vdots & \vdots \\ X_{PV1}^N & X_{PV2}^N & X_{PV3}^N & X_{WT1}^N & \dots & X_{WT4}^N & X_{bes1}^N & X_{bes2}^N & X_{BG}^N \end{bmatrix} \tag{44}$$

$$\boldsymbol{P_{DG}^T} = \begin{bmatrix} \boldsymbol{P_{PV}^T} \\ \boldsymbol{P_{WT}^T} \\ \boldsymbol{P_{bes}^T} \\ \boldsymbol{P_{BG}^T} \end{bmatrix} \tag{45}$$

TABLE 5. Parameters of electrical devices.

Devices	substation ¥/kW	converter station (DC) ¥/kW	Breaker ¥/device	Rectifier/Inverter ¥/kW	tansformer ¥/device	Cable ¥/m
AC	300	1,000	20,000 (10kV)	800	150,000 (10kV)	330 (10kV)
DC	300	1,000	40,0000 (±10kV) 200,000 (±6kV)	800	500,000 (±10kV) 300,000 (±6kV)	130 (±10kV)

TABLE 6. The number of different electronic devices and length of cabled in the micro-grid.

Devices	AC Micro-grid	DC Micro-grid	Hybrid Micro-grid
Breaker(AC)	1(BG)+N_{WT}+3(Load)+1 (PV+BES)	0	1(BG)+N_{WT}+2(AC Load)+1 (converter station)
Breaker(DC)	0	1(BG)+1 (WT) +3(Load)+1 (PV+BES)	1(DC Load)+1 (PV+BES)
Tansformer (AC)	1(BG)+N_{WT}+3(Load)+1 (PV+BES)	0	1(BG)+N_{WT}+2(AC Load)
Tansformer (DC)	0	1(DC Load)+1 (PV+BES)	1(DC Load)+1 (PV+BES)
Rectifier	$P_{BG} + N_{WT}.* P_{WT} + P_{\text{DC\_load}}$	$P_{BG} + N_{WT}.* P_{WT}$	$P_{BG} + N_{WT}.* P_{WT}$
Inverter	$P_{BG} + N_{WT}.* P_{WT} + N_{Pv}.* P_{PV}$	$P_{\text{AC\_load}}$	$P_{BG} + N_{WT}.* P_{WT}$
Bidirectional Converter	$N_{BES}.* P_{BES}$	0	Max ($P_{BG} + N_{WT}.* P_{WT}$, $N_{Pv}.* P_{PV} + N_{BES}.* P_{BES}$)
AC Cable (10kV)	1000m	0	1000* (P_{AC}/P_{total}) m
DC Cable (±10kV)	0	1000m	1000* (P_{DC}/P_{total}) m

The calling function ***calculatetime***() or ***calculatetimed***() in Algorithm 2 not only returns the operating status of RE, but also calculates and updates the state of BES after charging and discharging.

There are three situations of BES with charging state. First, only one type of battery satisfies the charging conditions. Secondly, both batteries meet the charging conditions. Thirdly, all the batteries do not satisfy the charging conditions. The programming process of charging of BES utilizes the '*xor*' function in MATLAB to estimate charging conditions, which is shown in Algorithm 3.

The calling function ***calculatetime***() is triggered while BES receives the signal for charging. This program assumes that the initial operating states of the two batteries in BES keep running and the values are set as 1 (true). When the battery satisfies the charging conditions, the value in ***OP*** extracts the corresponding value in $\boldsymbol{OP}_{ini}$ directly. Oppositely, the value of the in the ***OP*** is flipped from 1 to 0 when the battery does not satisfy the charging conditions. The SOC of the two batteries must be updated immediately at every moment. Especially, the function ***renewablelimitation***() is called when the output power of RE has a power reduction. Some RE stop running, and the values of equipment in the ***OP*** are flipped 1→0.

The BES discharges as the total output of RE and BG are unable to meet the load demand. The discharging situation of BES is similar to the charging situation. When the BES meets the discharging conditions whereas it cannot meet the power shortage of the load. Therefore, using the '||' function in MATLAB is for selecting the battery with discharge conditions. This method aims to ensure the battery discharges as much as possible for reducing the power shortage of the load. At the same time, the program modifies the status values of BES in ***OP*** and calculates LPSP. Moreover, no LPSP exists in ***Step1*** and ***Step2***, which is recorded as 0. In ***Step3***, the output of RE, BG, and BES is unable to meet the load, hence $LPSP > 0$.

VII. SIMULATION RESULTS AND DISCUSSIONS

A. CONVERGENCE OF OPTIMAL VALUE

Hyper plane and normalization methods are utilized before the end of iteration during simulation. The values in hyper plane are the contraction of actual values. Thus, following figures draw the plane with average values (Figure 10(a), (c), (e)) and maximum values (Figure 10(b), (d), (f)) instead of hyper plane for better observation of actual optimal values. The spots in following figures indicate the objective values reflected from the combination of population.

It can be seen from the simulation results in Figure 11 that better performances have obvious convergence on system cost and LPSP. The average values and maximum values are sorted out in Table 7. Balancing the objective factors is fundamental to determine the combination of DGs. However, compared with the convergence of cost and LPSP, Figure 11 and Table 7 show that the GHG emissions have weak shrinkage. In the three types of micro-grids, the distributions of optimal values have similar characteristics. As the second-biggest power generation in the operating strategy of a micro-grid, BG is arranged to supply power when RE generations are with insufficient supply ability. Particularly, substantial costs of WT, PV, and BES result in the larger per-unit cost of generating electricity. Oppositely, the capacity of BG with lower power generation cost is increased. Therefore, the results of GHG are higher in some cases. Furthermore, the results of system cost and LPSP have better convergence because of the proportional tailor-made combinations of RE power generation and BES.

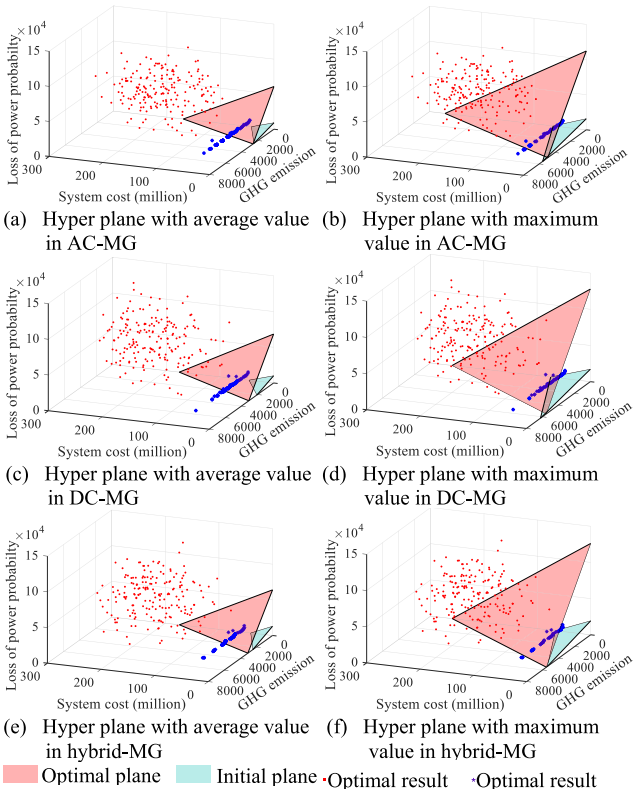

FIGURE 10. The simulation results.

TABLE 7. The average value and maximum value.

Type of MG	Type of Hyperplane	status	System cost	GHG emissions	LPSP
DC	Average	Initial	458.7	308	6884
		Optimal	175.86	208	1007
	Maximum	Initial	744.0	6239	127840
		Optimal	259.40	5510	17141
AC	Average	Initial	421.8	2594	60865
		Optimal	169.31	2485	9198
	Maximum	Initial	632.4	5572	112043
		Optimal	270.29	4910	15711
Hybrid	Average	Initial	406.5	3066	63922
		Optimal	173.71	2442	12892
	Maximum	Initial	659.5	5538	126168
		Optimal	259.65	5432	19279

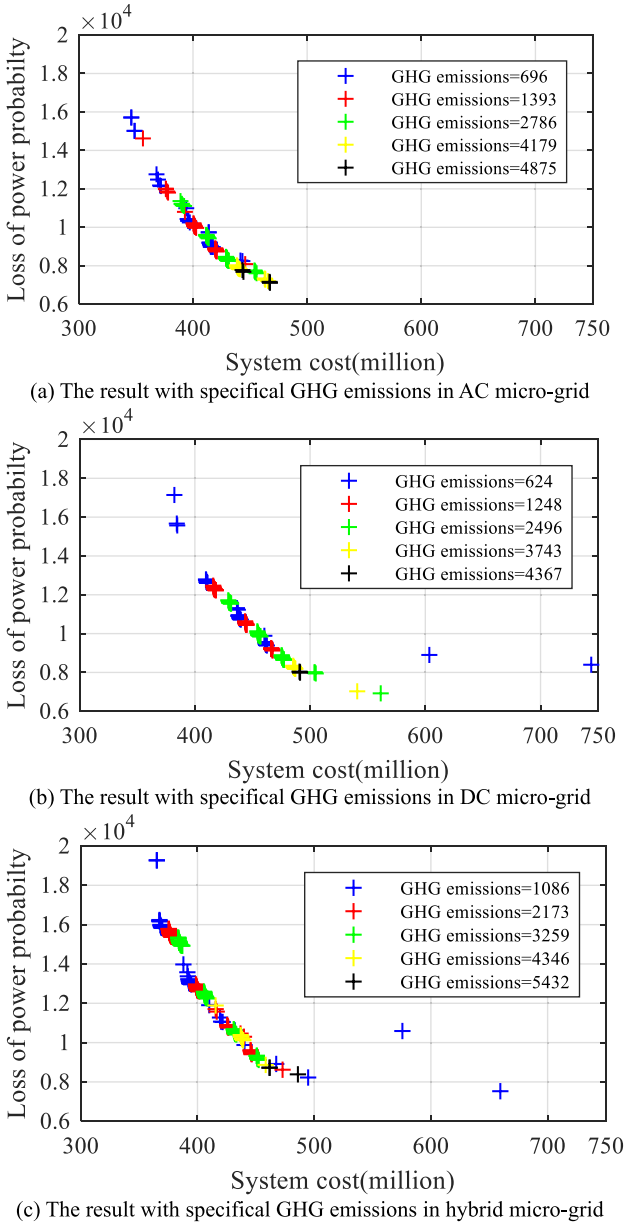

FIGURE 11. The distributions of results of system cost and LPSP when the value of GHG emissions are set equal to specific value.

B. RELATIONSHIPS BETWEEN OBJECTIVE FUNCTIONS

Figures 11 shows the distributions of results of system cost and LPSP when the values of GHG emissions are set equal to specifical value.

In Figures 11, it can be depicted that at the same GHG emissions, with the increase in the system cost, corresponding values of the LPSP decrease because the increase of system cost results in higher energy supplied by the DGs and lower possibility of power loss. Most results of system cost in the DC-MG focus between 400 and 500, whereas that in the AC-MG and hybrid MG mainly concentrate between 350 and 500. Moreover, some scattered results in DC micro-grid and hybrid micro-grid distribute far from the results group when the GHG emissions are situated in smaller values. Although these scattered results are far away from the results groups, it demonstrates that the diversity of optimal results. Actually, a lesser value of GHG emissions implies that the energy generated by the BG is smaller, further, the utilization of household waste is smaller. Additionally, the BG has better stability of energy supply than that of PV and WT because of its operation unimpeded by the environment, therefore, the higher energy supplied by the BG contributes to the less LPSP. With the growth of GHG emissions, the number of results hasa distinct reduction in Figures 11. Meanwhile, system costs concentrate gradually as the GHG emissions increase, for example, most results of system cost in hybrid MG are between 350 and 500 when the GHG emissions

TABLE 8. The value of IGD in DC, AC and hybrid micro-grid.

Type of MG	AC	DC	Hybrid
IGD	8718.293	9254.966	9659.24

are 1086. While the system costs shrink between 420 and 470 when the GHG emissions are 4346. Particularly, the concentration of system costs moves down slightly. This is because larger capacity of BG is installed and the inputs of other DGs get smaller in MG when the GHG emissions increase, and the results of total system cost tend to be similar.

C. INVERTED GENERATIONAL DISTANCE

Inverted Generational Distance (*IGD*) is an evaluation index with comprehensive performance. It calculates the sum of minimum distances between each point on the real Pareto frontier and the sets of individuals obtained by the algorithm so that it evaluates the convergence performance and distribution performance of the algorithm. The smaller the value of *IGD*, the better the comprehensive performance of the algorithm. The function of *IGD* is expressed as [40]:

$$IGD\,(P, Q) = \frac{\sum_{v \in P} d(v, Q)}{|P|} \tag{53}$$

where P is the sets of individuals distributed on the real Pareto surface, $|P|$ is the number of individuals,Q is the sets of optimal Pareto solutions obtained by the algorithm. $d(v, Q)$ represents the minimum Euclidean distance from individual$v$ in P to population Q.

In Table 8, the value of *IGD* is the smallest in the AC micro-grid, which is approximately 8718. However, the *IGD* is the largest in the hybrid micro-grid, which is about 9659. Therefore, the optimal simulation solutions in the AC-MG show the best convergence performance, but the optimal simulation solutions of the hybrid micro-grid underachieved in convergence performance. At the same time, the simulation solutions in the DC-MG perform mediocrely. In addition, the results of *IGD* are proved in Table 7, the system cost, LPSP, and GHG of AC-MG have obviously low values than other kinks of MGs.

D. COMPARATIVE ANALYSIS

In order to make comparisons between the sets of objective functions of different DGs combinations in DC-MG, AC-MG, and hybrid MG, Figure 12 shows the solutions in different colors.

Most solutions of objective functions in AC-MG are lower than that for DC-MG and hybrid MG. The reason is that the significant equipment applied to AC-MG has a long history of development, and they have developed into a mature technology. The prices of equipment are less than that for the DC-MG and hybrid MG. Solutions of objective functions in the hybrid MG are slightly lower than DC-MG and some are interlaced, which means these solutions in the DC-MG and hybrid MG might have similar system cost, LPSP and capacity of BG. Although part of the hybrid MG is composed of AC-MG

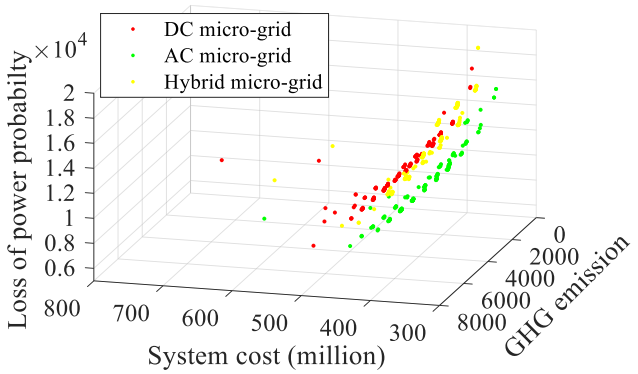

FIGURE 12. The solutions of DC, AC and hybrid micro-grid.

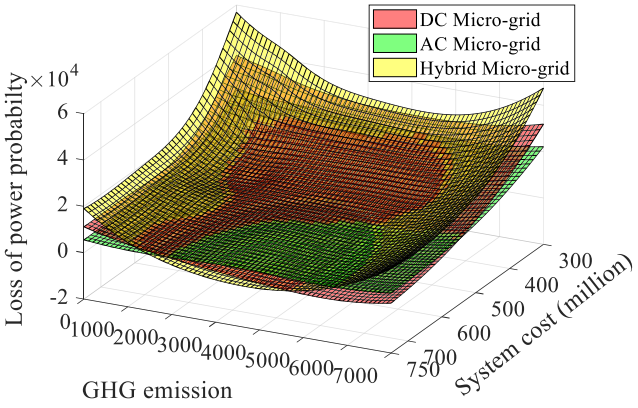

FIGURE 13. The surface fitting model of DC, AC and hybrid micro-grid solutions.

with lower system cost, the system cost of the hybrid MG keeps higher because of the expensive bidirectional converters. Figure 12 also confirms that the AC-MG has an excellent convergence performance with the lowest *IGD*.

An obvious limitation of this simulation is that the number of population cannot be set as large as possible, which reduces some potential solutions with special characteristics. In order to extend the solution space, the surface fitting model is emulated by using acquired combinations in the DC-MG, AC-MG, and hybrid micro-grid, which is shown in Figure 13.

It can be found that intersections and different forms of overlaps are shown in Figure 13. At the edge of objectives, it reveals the specific comparisons differ from the analysis above, for example, with the increase of system costs, the results of LPSP have two situations as the GHG emissions loop around 6000. When system cost is over about 550, the LPSPs of the hybrid micro-grid are greater than that of the AC micro-grid, further, the LPSPs of the AC micro-grid are greater than that of the DC micro-grid. Oppositely, when system costs less than about 550, the LPSPs of the hybrid micro-grid are larger than that of the DC micro-grid, and the LPSPs of the DC micro-grid are larger than that of the AC micro-grid.

It is difficult to observe the relationship of overlaps in the middle area in Figure 13. Figure 14 shows the top view

TABLE 9. The value of 9 cases.

Area	relationship of opverlap in LPSP
A	hybrid micro-grid>DC micro-grid>AC micro-grid
B	DC micro-grid>hybrid micro-grid>AC micro-grid
C	DC micro-grid>AC micro-grid>hybrid micro-grid
d	hybrid micro-grid>AC micro-grid>DC micro-grid
e	AC micro-grid>hybrid micro-grid>DC micro-grid
f	AC micro-grid>DC micro-grid>hybrid micro-grid

TABLE 10. The relationship of overlap in LPSP between DC, AC and hybrid micro-grid.

Case No.	Typy of Micro-grid	System cost	GHG emissions	LPSP	area
1	AC	632.44	3482.42	6665.88	f
2	AC	366.3	2089.45	14147.19	b
3	AC	441.59	696.48	8272.33	a
4	DC	561.3	2496	6923	c
5	DC	415.9	1248	12471	b
6	DC	513.1	6239	7390	a
7	hybrid	494.82	1086.47	8224.66	a
8	hybrid	458.44	4345.9	8866.07	b
9	hybrid	376.4	2172.95	15532.49	b

of Figure 13 and indicates the relationship of overlaps with different colors. Figure 14 is separated into six areas by differ colors. Differ areas denotes the different overlapping relationships of LPSP among the DC-MG, AC-MG, and hybrid MG at the same GHG emissions and system cost. It can be observed that the overlaps have no change when system costs are around 300 and GHG emissions are about 0. A slight change appears as the GHG emissions achieve approximately 7000. Especially, lots of changes are raised in the middle of the pattern and the end of GHG emissions. Accordingly, Table 9 indicates the relationships in different areas.

Factually, most solutions are distributed in areas a, b and c, and f. Therefore, the solutions in areas a, b, and c are the primary choice for selecting suitable solutions when the LPSP is as low as possible. In order to find the property and typical combination of DGs in AC-MG, DC-MG, and hybrid MG, we mapped Figure 12 into Figure13, and find the lower points in the three-objective space. Comparisons based

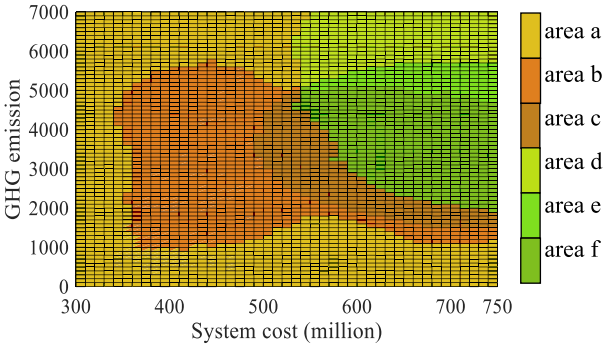

FIGURE 14. The top view of Figure 13.

upon system cost, GHG emissions, and LPSP, nine possible solutions chosen from the solution space are tabulated in Table 10. The corresponding optimal capacities of PV, WT, BES, and BG are listed in Table 11.

In Table 10, system cost is minimum in Case 2 and maximum in Case 1, as can be seen in Table 11 that the installed capacities of DGs in AC-MG of Case 1 are greater than that of other cases. This enhances the total system cost in Case 1. However, the capacities of most DGs in Case 2 are lower than other cases, which decreases the cost of power electronic devices in Case 2. In Table 10, the values of GHG emissions are smaller in Case 3 and Case 7, whilst they are larger in Case 6 and 8, and moderate for other Cases. Table 11 shows that only one BG machine is utilized in Cases 3 and 7, there is the reason that these cases represent lower GHG emissions. While Case 6 installs the largest capacity of BG among the 9 cases. Although Case 8 only has 20kW of BG, the explanation is that the BG in Case 8 has with longer operating time. Additionally, Table 10 shows that LPSPs are highest for Cases 2 and 9 whereas lower for Case 4 and Case 6, and lowest for Case 1, because the installed capacities of DGs in Cases 1, 4, and 6 are higher than that of other cases (Table 11).

As the optimal solution is determined based upon the mentioned objectives, Table 10 clearly shows that Case 3 is the optimal choice. Although the system costs are lower in Case 2 and Case 9, they are not be selected due to the relatively higher insufficient power supply. The LPSPs of the Case 2 and Case 9 are around 70% and 87% larger than that

TABLE 11. The combination of DGs in 9 cases.

Case No.	PV1 kW	PV2 kW	PV3 kW	WT1 kW	WT2 kW	WT3 kW	WT4 kW	BES1 kWh	BES2 kWh	BG kW
1	0	0	77.1	220	750	1320	1000	0.48	66	50
2	0	0	75.3	110	250	330	1000	18.84	0	30
3	0	0	72.9	110	500	1320	1000	0.48	0	10
4	0.3	0.3	91.5	110	1000	1320	1000	0.48	0	40
5	0.3	0.3	91.2	110	250	660	1000	1.2	0	20
6	0.3	0.3	69	110	250	1320	1000	0.24	38	100
7	0.3	0	72.3	110	250	330	1000	0.48	0	10
8	117.6	18.6	373.5	110	500	330	1000	0.48	0	20
9	0.3	0	108.3	110	250	330	1000	0.48	104	20

of Case 3 respectively. Case 1 has the largest system cost and GHG emissions which are about 43.2% and 5 times greater than Case 3 separately. Moreover, the LPSPs in Case 4 and Case 6 are 16.3% and 10.7% less than Case 3, but the system costs in Case 4 and Case 6 are 27.1% and 16.2% larger than that in Case 3, and the GHG emissions in Case 4 and Case 6 are around 3 times larger and 9 times than that in Case 3. Compared with Case 3, Case 5's system cost has less system cost, but the values of GHG emissions and LPSP in Case 5 are quite higher than Case 3 which are 1.8 times and 50.8% higher than Case 3.

Through the four ways of analysis including extremum and average value, *IGD*, the surface fitting model, and comparison, we found that AC-MG is the most suitable microgrid structure in this location. And then, a relatively reasonable DG capacity allocation of AC-MG comes out. Therefore, it is certain that this method can achieve the purpose we proposed that finding the befitting structure of MG and corresponding combination of DGs that less other works mentioned.

Algorithm 1 DGs' Annual $\boldsymbol{OP_{ini}}$ With 0.1 Step

read: $PV\ Wind\ N_{PV}\ N_{WT}\ N_{bes}$
for $t = 1:1:8760/0.1$
  if $PV\ (t) > 0$
    $OP_{PV}\ (1,t) = 1;$
  else
    $OP_{PV}\ (1,t) = 0;$
  end
  if $(Wind\ (t) >= 2.8)\ \&\&\ (Wind\ (t) <= 25)$
    $OP_{WT}\ (1,t) = 1;$
  else
    $OP_{WT}\ (1,t) = 0;$
  end
if $(Wind\ (t) >= 3)\ \&\&\ (Wind\ (t) <= 25)$
    $OP_{WT}\ (2,t) = 1;$
  else
    $OP_{WT}\ (2,t) = 0;$
  end
$OP_{PV\_total} = \boldsymbol{repmat}(OP_{PV}, N_{PV}, 1);$
$OP_{WT\_total} = [OP_{WT}\ (1,:); \boldsymbol{repmat}(OP_{WT}(2,:), N_{wt}-1, 1)];$
$OP_{bes} = \boldsymbol{ones}(1, \text{size}(0{:}0.1{:}8760, 2));$
$OP_{bes\_total} = \boldsymbol{repmat}(OP_{bes}, N_{bes}, 1);$
$OP_{BG} = \boldsymbol{ones}(1, \text{size}(0{:}0.1{:}8760, 2));$
$OP_{BG\_total} = \boldsymbol{repmat}(OP_{BG}, N_{BG}, 1);$
$\boldsymbol{OP_{ini}} = [OP_{PV\_total}; OP_{WT\_total}; OP_{bes\_total}; OP_{BG\_total}];$
end

VIII. CONCLUSION

This paper used the case study of Kongtong island to select a suitable type of islanded micro-grid from DC-MG, AC-MG, and hybrid MG, and find an associated DGs' configuration. This investigation is primarily dependent upon multiple important objectives associated with a micro-grid system including system cost minimization, less greenhouse gas (GHG) emissions, and higher reliability. In order to improve the accuracy of simulation results, the proposed method estimated uncertainties in residential power demand, solar irradiation, temperature, and wind speed data. In a micro-grid, the DGs are comprised of wind turbine (WT), solar photovoltaic (PV), battery energy storage (BES) system, and biomass power generation (BG). The uncertainties caused by power electronic devices are considered for calculating accurate system cost of each kind of micro-grid. The NSGA-III algorithm is applied for the multi-objective problem. It has been also observed that the AC-MG is the optimal choice for Kongtong Island with multiple analyses including the advantages extremum and average values, *IGD*, the surface fitting model, and comparison. Moreover, it is

Algorithm 2 Running Time of Each DGs

for n=1:N
for t = 1:8760/0.1
read: $SOC1\ (t)\ , SOC2\ (t)\ , P_{BG}^{max},\ P_{BG}^{min},\ N_{PV},\ N_{WT},\ PV,$ $TempWind$
calculate: $P_{PV}\ (t), P_{WT}\ (t), P_{bes}\ (t), P_{BG}\ (t)$
$P_{ren}\ (t) = P_{PV}\ (t) + P_{WT}\ (t)$
if $P_{ren}\ (t) > P_{load}\ (t)$
  $\Delta P = P_{ren}\ (t) - P_{load}\ (t)$
  $[T_{PV\_on}, T_{WT\_on}, T_{bes\_on}]$=**calculatetime()**
  update: $SOC1\ (t)\ SOC2\ (t)$
$T_{BG\_on} = \text{false}$
$P_{vac}\ (t) = 0$
elseif$(P_{ren}\ (t) < P_{load}\ (t))\ \&\&(P_{ren}\ (t) + P_{BG}\ (t) > P_{load}\ (t))$
  if $\left(P_{ren}\ (t) + P_{BG}^{min} < P_{load}\ (t)\right)$
  $\&\&\ \left(P_{ren}\ (t) + P_{BG}^{max} > P_{load}\ (t)\right)$
    update: $SOC1\ (t)\ SOC2\ (t)$
$OP(N_{PV} + N_{WT} + 1, t) = \text{false}$
$OP(N_{PV} + N_{WT} + 2, t) = \text{false}$
$T_{PV\_on} = OP(1 : N_{PV}, t)'$
$T_{WT\_on} = OP(N_{PV} + 1 : N_{PV} + N_{WT}, t)'$
$T_{bes\_on} = OP(N_{PV} + N_{WT} + 1 : N_{PV} + N_{WT} + N_{bes}, t)'$
elseif $P_{ren}\ (t) + P_{BG}^{min} > P_{load}\ (t)$
$[T_{PV\_on}, T_{WT\_on}, T_{bes\_on}]$= **calculatetime()**
  update: $SOC1\ (t)\ SOC2\ (t)$
end
$T_{BG\_on} = \text{true}$
$P_{vac}\ (t) = 0$
elseif$P_{ren}\ (t) + P_{BG}^{max} < P_{load}\ (t)$
  $[T_{PV\_on}, T_{WT\_on}, T_{bes\_on}, P_{vac}(t)]$= **calculatetimed()**
  update: $SOC1\ (t)\ SOC2\ (t)$
$T_{BG\_on} = \text{true}$
  end
$T_{on} = [T_{PV\_on}; T_{WT\_on}; T_{bes\_on}; T_{BG\_on}]$
  $\text{LPSP}(t) = P_{vac}(t)/P_{load}\ (t)$
if t == 8760/0.1
  $T_{total}(n,:) = sum(T_{on})$
  LPSP$t(n,:)$ =sum(LPSP)
end

also accompanied by the optimal combinations of DGs. The case study confirms that these uncertainties and multiple analyses methods can be considered in other places where the people plan to construct a micro-grid. These uncertainties and analyses methods are beneficial to achieve an accurate combination of DGs in an MG.

Algorithm 3 Charging Process of BES

$[T_{PV\_on}, T_{WT\_on}, T_{bes\_on}]$=**calculatetime()**
read: $P_{bes1}(n)\ P_{bes2}(n)\ P_{ch}\ N_{PV} N_{WT} N_{bes} SOC1\ (t)\ SOC2\ (t)$
U=**xor**$((SOC1(t) <= SOC1^{max} \&\& \Delta P(t) < P_{bes1}(n) * P_{ch}), (SOC2(t) <= SOC2^{max} \&\& \Delta P(t) < P_{bes2}(n) * P_{ch}))$
if U==1
  if $(SOC1(t) <= SOC1^{max} \&\& \Delta P(t) < P_{bes1}(n) * P_{ch})$ ==true
    $SOC1(t+1) = SOC1(t) + 0.1 * \Delta P(t) * P_{bes1}(n)/0.7$
    $OP\ (N_{PV} + N_{WT} + 1, t)$ ==true
  else
    $SOC1(t+1) = SOC1(t)$
    $OP\ (N_{PV} + N_{WT} + 1, t)$ == false
  end
  if $(SOC2(t) <= SOC2^{max} \&\& \Delta P(t) < P_{bes2}(n) * P_{ch})$ ==true
    $SOC2(t+1) = SOC2(t) + 0.1 * \Delta P(t) * P_{bes2}(2)/0.9$
    $OP\ (N_{PV} + N_{WT} + 2, t)$ =true
  else
    $SOC1(t+2) = SOC1(t)$
    $OP\ (N_{PV} + N_{WT} + 2, t)$ == false
  end
$T_{bes\_on} = OP(N_{PV} + N_{WT} + 1 : N_{PV} + N_{WT} + N_{bes}, t)'$
$T_{PV\_on} = OP(1 : N_{PV}, t)'$
$T_{WT\_on} = OP(N_{PV} + 1 : N_{PV} + N_{WT}, t)'$
elseif $[(SOC1(t) <= SOC1^{max}) \&\& (\Delta P(t) < P_{bes1}(n) * P_{ch})]$
$\&\&[(SOC2(t) <= SOC2^{max}) \&\& [(\Delta P(t) < P_{bes2}(n) * P_{ch})]$
update: $SOC1\ (t)\ SOC2\ (t)$
$P(N_{PV} + N_{WT} + 1, t) = ture$
$OP(N_{PV} + N_{WT} + 2, t) = ture$
$T_{PV\_on} = OP(1 : N_{PV}, t)'$
$T_{WT\_on} = OP(N_{PV} + 1 : N_{PV} + N_{WT}, t)'$
$T_{bes\_on} = OP(N_{PV} + N_{WT} + 1 : N_{PV} + N_{WT} + N_{bes}, t)'$
else
update: $SOC1\ (t)\ SOC2\ (t)$
$OP(N_{PV} + N_{WT} + 1, t) = false$
$OP(N_{PV} + N_{WT} + 2, t) = false$
$T_{bes\_on} = OP(N_{PV} + N_{WT} + 1 : N_{PV} + N_{WT} + N_{bes}, t)'$
  $[T_{PV\_on}, T_{WT\_on}]$=**renewablelimitation()**
end

It has two problems during our research. Firstly, the NSGA-III algorithm has a complex computational process and spent a long time to compute on MATLAB platform. Secondly, the nine cases are chosen by authors' observation and subjectivity. For future work, our authors will take into account more comprehensive factors such as land area, Direct Normal Irradiance (DNI), or Diffuse Horizontal Irradiance (DHI) of PV system, and improve the NSGA-III algorithm to enhance the performance in more complex simulation environments. In addition, the evaluation method of results should be improved in the next work for selecting the suitable micro-grid structure and DGs' configuration.

APPENDIX

See Algorithms 1–3.

REFERENCES

[1] X. Xu, W. Hu, D. Cao, Q. Huang, C. Chen, and Z. Chen, "Optimized sizing of a standalone PV-wind-hydropower station with pumped-storage installation hybrid energy system," *Renew. Energy*, vol. 147, pp. 1418–1431, Mar. 2020.
[2] S. Mazzola, M. Astolfi, and E. Macchi, "The potential role of solid biomass for rural electrification: A techno economic analysis for a hybrid microgrid in India," *Appl. Energy*, vol. 169, pp. 370–383, May 2016.
[3] S. M. Cai, "Discussion on the main problems and countermeasures of the environmental protection facilities such as desulfuration in thermal power plants," *Manage. Technol. SME*, vol. 9, pp. 141–142, Sep. 2018.
[4] A. Raghavan, P. Maan, and A. K. B. Shenoy, "Optimization of day-ahead energy storage system scheduling in microgrid using genetic algorithm and particle swarm optimization," *IEEE Access*, vol. 8, pp. 173068–173078, 2020.
[5] J. Firestone, A. W. Bates, and A. Prefer, "Power transmission: Where the offshore wind energy comes home," *Environ. Innov. Societal Transitions*, vol. 29, pp. 90–99, Dec. 2018.
[6] J. A. A. Silva, J. C. López, N. B. Arias, M. J. Rider, and L. C. P. da Silva, "An optimal stochastic energy management system for resilient microgrids," *Appl. Energy*, vol. 300, Oct. 2021, Art. no. 117435.
[7] A. S. O. Ogunjuyigbe, T. R. Ayodele, and O. A. Akinola, "Optimal allocation and sizing of PV/wind/split-diesel/battery hybrid energy system for minimizing life cycle cost, carbon emission and dump energy of remote residential building," *Appl. Energy*, vol. 171, pp. 153–171, Jun. 2016.
[8] A. A. Hamad, M. E. Nassar, E. F. El-Saadany, and M. M. A. Salama, "Optimal configuration of isolated hybrid AC/DC microgrids," *IEEE Trans. Smart Grid*, vol. 10, no. 3, pp. 2789–2798, May 2019.
[9] V. V. V. S. N. Murty and A. Kumar, "Optimal energy management and techno-economic analysis in microgrid with hybrid renewable energy sources," *J. Mod. Power Syst. Clean Energy*, vol. 8, no. 5, pp. 929–940, Sep. 2020.
[10] M. A. Mosa and A. A. Ali, "Energy management system of low voltage DC microgrid using mixed-integer nonlinear programing and a global optimization technique," *Electr. Power Syst. Res.*, vol. 192, Mar. 2021, Art. no. 106971.
[11] P. Wang, W. Wang, and D. Xu, "Optimal sizing of distributed generations in DC microgrids with comprehensive consideration of system operation modes and operation targets," *IEEE Access*, vol. 6, pp. 31129–31140, 2018.
[12] H. X. Yang, W. Zhou, L. Lu, and Z. Fang, "Optimal sizing method for stand-alone hybrid solar-wind system with LPSP technology by using genetic algorithm," *Sol. Energy.*, vol. 82, no. 4, pp. 354–367, 2008.
[13] M. B. Shadmand and R. S. Balog, "Multi-objective optimization and design of photovoltaic-wind hybrid system for community smart DC microgrid," *IEEE Trans. Smart Grid*, vol. 5, no. 5, pp. 2635–2643, Sep. 2014.
[14] B. Zhao, X. Zhang, J. Chen, C. Wang, and L. Guo, "Operation optimization of standalone microgrids considering lifetime characteristics of battery energy storage system," *IEEE Trans. Sustain. Energy*, vol. 4, no. 4, pp. 934–943, Oct. 2013.
[15] A. Das and Z. Ni, "A computationally efficient optimization approach for battery systems in islanded microgrid," *IEEE Trans. Smart Grid*, vol. 9, no. 6, pp. 6489–6499, Nov. 2018.
[16] P. Li, R.-X. Li, Y. Cao, D.-Y. Li, and G. Xie, "Multiobjective sizing optimization for island microgrids using a triangular aggregation model and the Levy-harmony algorithm," *IEEE Trans. Ind. Informat.*, vol. 14, no. 8, pp. 3495–3505, Aug. 2018.
[17] M. Kharrich, O. H. Mohammed, N. Alshammari, and M. Akherraz, "Multi-objective optimization and the effect of the economic factors on the design of the microgrid hybrid system," *Sustain. Cities Soc.*, vol. 65, Feb. 2021, Art. no. 102646.

[18] H. Moradi, M. Esfahanian, A. Abtahi, and A. Zilouchian, "Modeling a hybrid microgrid using probabilistic reconfiguration under system uncertainties," *Energies*, vol. 10, no. 9, p. 1430, Sep. 2017.

[19] S. Mohamed, M. F. Shaaban, M. Ismail, E. Serpedin, and K. A. Qaraqe, "An efficient planning algorithm for hybrid remote microgrids," *IEEE Trans. Sustain. Energy*, vol. 10, no. 1, pp. 257–267, Jan. 2019.

[20] A. M. Ferrario, A. Bartolini, F. Segura Manzano, F. J. Vivas, G. Comodi, S. J. McPhail, and J. M. Andujar, "A model-based parametric and optimal sizing of a battery/hydrogen storage of a real hybrid microgrid supplying a residential load: Towards island operation," *Adv. Appl. Energy*, vol. 3, Aug. 2021, Art. no. 100048.

[21] A. A. Abdelsalam, H. A. Gabbar, and A. M. Sharaf, "Performance enhancement of hybrid AC/DC microgrid based D-FACTS," *Int. J. Electr. Power Energy Syst.*, vol. 63, pp. 382–393, Dec. 2014.

[22] A. K. Basu, A. Bhattacharya, S. Chowdhury, and S. P. Chowdhury, "Planned scheduling for economic power sharing in a CHP-based microgrid," *IEEE Trans. Power Syst.*, vol. 27, no. 1, pp. 30–38, Feb. 2012.

[23] M. A. Hassan and M. A. Abido, "Optimal design of microgrids in autonomous and grid-connected modes using particle swarm optimization," *IEEE Trans. Power Electron.*, vol. 26, no. 3, pp. 755–769, Mar. 2011.

[24] U. Asgher, M. Rasheed, A. Al-Sumaiti, A. Rahman, I. Ali, A. Alzaidi, and A. Alamri, "Smart energy optimization using heuristic algorithm in smart grid with integration of solar energy sources," *Energies*, vol. 11, no. 12, p. 3494, Dec. 2018.

[25] M. S. Ismail, M. Moghavvemi, and T. M. I. Mahlia, "Genetic algorithm based optimization on modeling and design of hybrid renewable energy systems," *Energy Convers. Manage.*, vol. 85, pp. 120–130, Sep. 2014.

[26] M. Mohammadi, S. H. Hosseinian, and G. B. Gharehpetian, "GA-based optimal sizing of microgrid and DG units under pool and hybrid electricity markets," *Int. J. Electr. Power Energy Syst.*, vol. 35, no. 1, pp. 83–92, Feb. 2012.

[27] H. U. R. Habib, U. Subramaniam, A. Waqar, B. S. Farhan, K. M. Kotb, and S. R. Wang, "Energy cost optimization of hybrid renewables based V2G microgrid considering multi objective function by using artificial bee colony optimization," *IEEE Access*, vol. 8, pp. 62076–62093, 2020.

[28] M. Juneja, S. K. Nagar, and S. R. Mohanty, "ABC based reduced order modelling of microgrid in grid-tied mode," *Control Eng. Pract.*, vol. 84, pp. 337–348, Mar. 2019.

[29] M. Marzband, E. Yousefnejad, and A. Sumper, "Real time experimental implementation of optimum energy management system in standalone microgrid by using multi-layer ant colony optimization," *Int. J. Elect. Power Energy Syst.*, vol. 75, pp. 265–274, Feb. 2016.

[30] D. Dabhi and K. Pandya, "Uncertain scenario based MicroGrid optimization via hybrid levy particle swarm variable neighborhood search optimization (HL_PS_VNSO)," *IEEE Access*, vol. 8, pp. 108782–108797, 2020.

[31] L. Zhang, H. Zheng, Q. Hu, B. Su, and L. Lyu, "An adaptive droop control strategy for islanded microgrid based on improved particle swarm optimization," *IEEE Access*, vol. 8, pp. 3579–3593, 2020.

[32] M. Marzband, F. Azarinejadian, M. Savaghebi, and J. M. Guerrero, "An optimal energy management system for islanded microgrids based on multiperiod artificial bee colony combined with Markov chain," *IEEE Syst. J.*, vol. 11, no. 3, pp. 1712–1722, Sep. 2017.

[33] A. O. Rousis, I. Konstantelos, and G. Strbac, "A planning model for a hybrid AC–DC microgrid using a novel GA/AC OPF algorithm," *IEEE Trans. Power Syst.*, vol. 35, no. 1, pp. 227–237, Jan. 2020.

[34] A. Askarzadeh, "A memory-based genetic algorithm for optimization of power generation in a microgrid," *IEEE Trans. Sustain. Energy*, vol. 9, no. 3, pp. 1081–1089, Jul. 2018.

[35] Z. Bao, Q. Zhou, Z. Yang, Q. Yang, L. Xu, and T. Wu, "A multi time-scale and multi energy-type coordinated microgrid scheduling solution—Part II: Optimization algorithm and case studies," *IEEE Trans. Power Syst.*, vol. 30, no. 5, pp. 2267–2277, Sep. 2015.

[36] M. H. Moradi and M. Eskandari, "A hybrid method for simultaneous optimization of DG capacity and operational strategy in microgrids considering uncertainty in electricity price forecasting," *Renew. Energy*, vol. 68, pp. 697–714, Aug. 2014.

[37] K. Roy, K. K. Mandal, A. C. Mandal, and S. N. Patra, "Analysis of energy management in micro grid—A hybrid BFOA and ANN approach," *Renew. Sustain. Energy Rev.*, vol. 82, pp. 4296–4308, Feb. 2018.

[38] K. Deb, A. Pratap, S. Agarwal, and T. Meyarivan, "A fast and elitist multiobjective genetic algorithm: NSGA-II," *IEEE Trans. Evol. Comput.*, vol. 6, no. 2, pp. 182–197, Aug. 2002.

[39] K. Deb and H. Jain, "An evolutionary many-objective optimization algorithm using reference-point-based nondominated sorting approach, Part I: Solving problems with box constraints," *IEEE Trans. Evol. Comput.*, vol. 18, no. 4, pp. 577–601, Aug. 2014.

[40] H. Jain and K. Deb, "An evolutionary many-objective optimization algorithm using reference-point based nondominated sorting approach, Part II: Handling constraints and extending to an adaptive approach," *IEEE Trans. Evol. Comput.*, vol. 18, no. 4, pp. 602–622, Aug. 2014.

[41] H. Ishibuchi, R. Imada, Y. Setoguchi, and Y. Nojima, "Performance comparison of NSGA-II and NSGA-III on various many-objective test problems," in *Proc. IEEE Congr. Evol. Comput. (CEC)*, Jul. 2016, pp. 3045–3052.

[42] J. H. Zheng, C. Q. Wu, J. Huang, Y. Liu, and Q. H. Wu, "Multi-objective optimization for coordinated day-ahead scheduling problem of integrated electricity-natural gas system with microgrid," *IEEE Access*, vol. 8, pp. 86788–86796, 2020.

[43] I. R. S. da Silva, R. de A. L. Rabêlo, J. J. P. C. Rodrigues, P. Solic, and A. Carvalho, "A preference-based demand response mechanism for energy management in a microgrid," *J. Cleaner Prod.*, vol. 255, May 2020, Art. no. 120034.

[44] C. D. Rodríguez-Gallegos, D. Yang, O. Gandhi, M. Bieri, T. Reindl, and S. K. Panda, "A multi-objective and robust optimization approach for sizing and placement of PV and batteries in off-grid systems fully operated by diesel generators: An Indonesian case study," *Energy*, vol. 160, pp. 410–429, Oct. 2018.

[45] W. Liu, C. Liu, Y. Lin, K. Bai, and L. Ma, "Interval multi-objective optimal scheduling for redundant residential microgrid with VESS," *IEEE Access*, vol. 7, pp. 87849–87865, 2019.

[46] C. Wang, Y. Liu, X. Li, L. Guo, L. Qiao, and H. Lu, "Energy management system for stand-alone diesel-wind-biomass microgrid with energy storage system," *Energy*, vol. 97, pp. 90–104, Feb. 2016.

[47] L. Guo, W. Liu, X. Li, Y. Liu, B. Jiao, W. Wang, C. Wang, and F. Li, "Energy management system for stand-alone wind-powered-desalination microgrid," *IEEE Trans. Smart Grid*, vol. 7, no. 2, pp. 1079–1087, Mar. 2016.

[48] L. Wen, K. Zhou, S. Yang, and X. Lu, "Optimal load dispatch of community microgrid with deep learning based solar power and load forecasting," *Energy*, vol. 171, pp. 1053–1065, Mar. 2019.

[49] E. S. Oda, A. M. A. E. Hamed, A. Ali, A. A. Elbaset, M. A. E. Sattar, and M. Ebeed, "Stochastic optimal planning of distribution system considering integrated photovoltaic-based DG and DSTATCOM under uncertainties of loads and solar irradiance," *IEEE Access*, vol. 9, pp. 26541–26555, 2021.

[50] M. Ebeed, A. Ali, M. I. Mosaad, and S. Kamel, "An improved lightning attachment procedure optimizer for optimal reactive power dispatch with uncertainty in renewable energy resources," *IEEE Access*, vol. 8, pp. 168721–168731, 2020.

[51] A. Ramadan, M. Ebeed, S. Kamel, A. Y. Abdelaziz, and H. H. Alhelou, "Scenario-based stochastic framework for optimal planning of distribution systems including renewable-based DG units," *Sustainability*, vol. 13, no. 6, p. 3566, Mar. 2021.

[52] U. Akram, M. Khalid, and S. Shafiq, "An innovative hybrid wind-solar and battery-supercapacitor microgrid system-development and optimization," *IEEE Access*, vol. 5, pp. 25897–25912, 2017.

[53] A. Khatibzadeh, M. Besmi, A. Mahabadi, and M. Reza Haghifam, "Multi-agent-based controller for voltage enhancement in AC/DC hybrid microgrid using energy storages," *Energies*, vol. 10, no. 2, p. 169, Feb. 2017.

[54] E. Skoplaki and J. A. Palyvos, "Operating temperature of photovoltaic modules: A survey of pertinent correlations," *Renew. Energy*, vol. 34, no. 1, pp. 23–29, Jan. 2009.

[55] O. Gandhi, C. D. Rodríguez-Gallegos, W. Zhang, D. Srinivasan, and T. Reindl, "Economic and technical analysis of reactive power provision from distributed energy resources in microgrids," *Appl. Energy*, vol. 210, pp. 827–841, Jan. 2018.

[56] B. Ye, X. Shi, X. Wang, and H. Wu, "Optimisation configuration of hybrid AC/DC microgrid containing electric vehicles based on the NSGA-II algorithm," *J. Eng.*, vol. 2019, no. 10, pp. 7229–7236, Oct. 2019.

[57] A. Fathy, K. Kaaniche, and T. M. Alanazi, "Recent approach based social spider optimizer for optimal sizing of hybrid PV/wind/battery/diesel integrated microgrid in aljouf region," *IEEE Access*, vol. 8, pp. 57630–57645, 2020.

[58] W. Y. M, Jianlong, L. Wenchun, and Z. X. Qilao, "Analysis of fatigue damage differences of blades under dynamic wind load," *J. Vib. Shock*, vol. 39, pp. 271–277, Dec. 2020.

XIAOXU MA received the B.S. degree from the University of Jinan, Jinan, China, in 2013, and the M.S. degree in energy and sustainability with electrical power engineering from the University of Southampton, U.K., in 2016. She is currently pursuing the Ph.D. degree with the School of Electrical Engineering, Shandong University, Jinan. Her current research interests include the operation and design and optimization of micro-grid, distributed energy resources, and energy storage systems.

SHUQIN LIU received the B.S. degree in electronic engineering from Shandong University, Jinan, China, in 1982, and the M.S. and Ph.D. degrees in electronic engineering and mechanical engineering from Xi'an Jiaotong University, Xi'an, China, in 1990 and 2000, respectively.

She is currently a Professor with the School of Electrical Engineering, Shandong University. Her research fields are Maglev flywheel energy storage system, application of the theory and technology of active magnetic bearing technology.

HONGTAO LIU is currently pursuing the Ph.D. degree in electrical engineering with Shandong University, Jinan, China. His research interests include physiological control, modeling, and simulation; and algorithm development with emphasis on left ventricular assist devices.

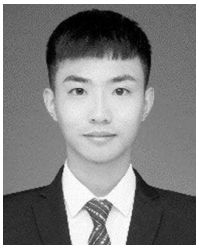

SIPENG ZHAO received the master's degree in electrical engineering from Shandong University, in 2020. He currently works with State Grid Liaocheng Power Supply Company. His research include magnetic levitation technology and live power distribution operations.